

Are breaking waves, bores, surges and jumps the same flow?

Pierre Lubin^{1,2} · Hubert Chanson²

Received: 26 July 2015 / Accepted: 21 July 2016 / Published online: 1 August 2016
© Springer Science+Business Media Dordrecht 2016

Abstract The flow structure in the aerated region of the roller generated by breaking waves remains a great challenge to study, with large quantities of entrained air and turbulence interactions making it very difficult to investigate in details. A number of analogies were proposed between breaking waves in deep or shallow water, tidal bores and hydraulic jumps. Many numerical models used to simulate waves in the surf zone do not implicitly simulate the breaking process of the waves, but are required to parameterise the wave-breaking effects, thus relying on experimental data. Analogies are also assumed to quantify the roller dynamics and the energy dissipation. The scope of this paper is to review the different analogies proposed in the literature and to discuss current practices. A thorough survey is offered and a discussion is developed aimed at improving the use of possible breaking proxies. The most recent data are revisited and scrutinised for the use of most advanced numerical models to educe the surf zone hydrodynamics. In particular, the roller dynamics and geometrical characteristics are discussed. An open discussion is proposed to explore the actual practices and propose perspectives based on the most appropriate analogy, namely the tidal bore.

Keywords Breaking waves · Breaking bores · Hydraulic jumps · Air bubble entrainment · Flow singularity · Tidal bores

1 Introduction

Surface wave breaking, occurring in the open ocean or the coastal zone, is a complex and challenging two-phase flow phenomenon which plays an important role in numerous processes, including air–sea transfer of gas, momentum and energy, and in a number of

✉ Pierre Lubin
p.lubin@i2m.u-bordeaux1.fr

¹ Université de Bordeaux, I2M, CNRS UMR 5295, 16 Avenue Pey-Berland, 33607 Pessac, France

² School of Civil Engineering, The University of Queensland, Brisbane, QLD 4072, Australia

technical applications such as acoustic underwater communications and optical properties of the water column. The major visible feature during wave breaking is the large quantities of air entrained in the form of bubble clouds and whitecaps, generally coined surface foam (Figs. 1, 2). The generation of bubble clouds has been shown to induce energy dissipation and turbulent mixing, to contribute to heat exchange and enhance gas transfer [94, 182]. Bubble clouds have been shown to influence climate and intensification of tropical cyclones [176], and cause the ocean ambient noise [148]. The breakup and evolution of entrained air into numerous bubbles is a source of acoustic noise, which is important for naval hydrodynamics. The hydrodynamic performance of ships is influenced by the wake

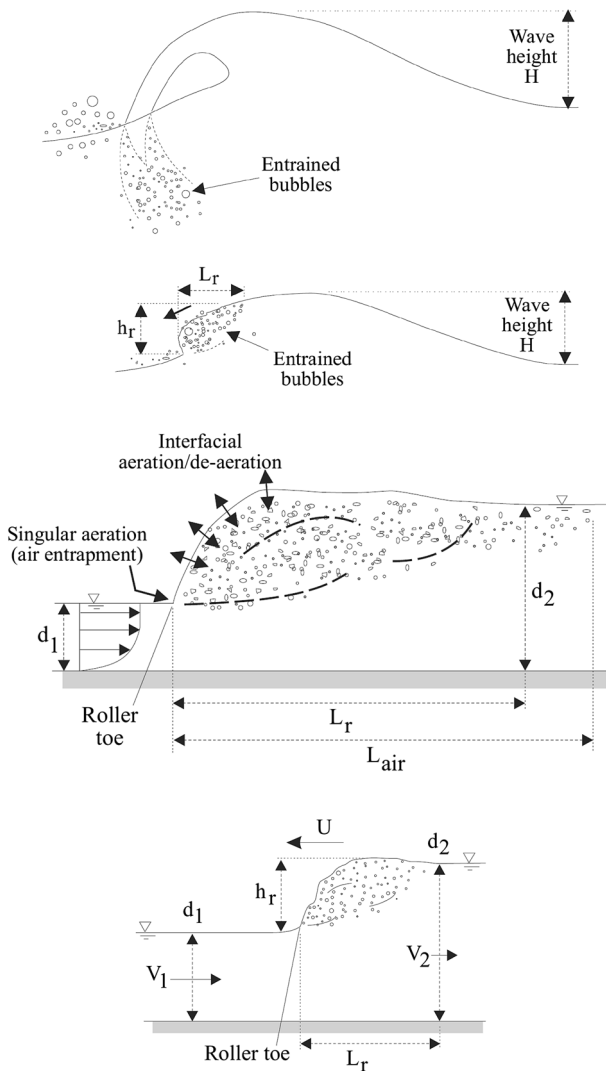


Fig. 1 Sketches of breaking waves, bore, roller and hydraulic jump

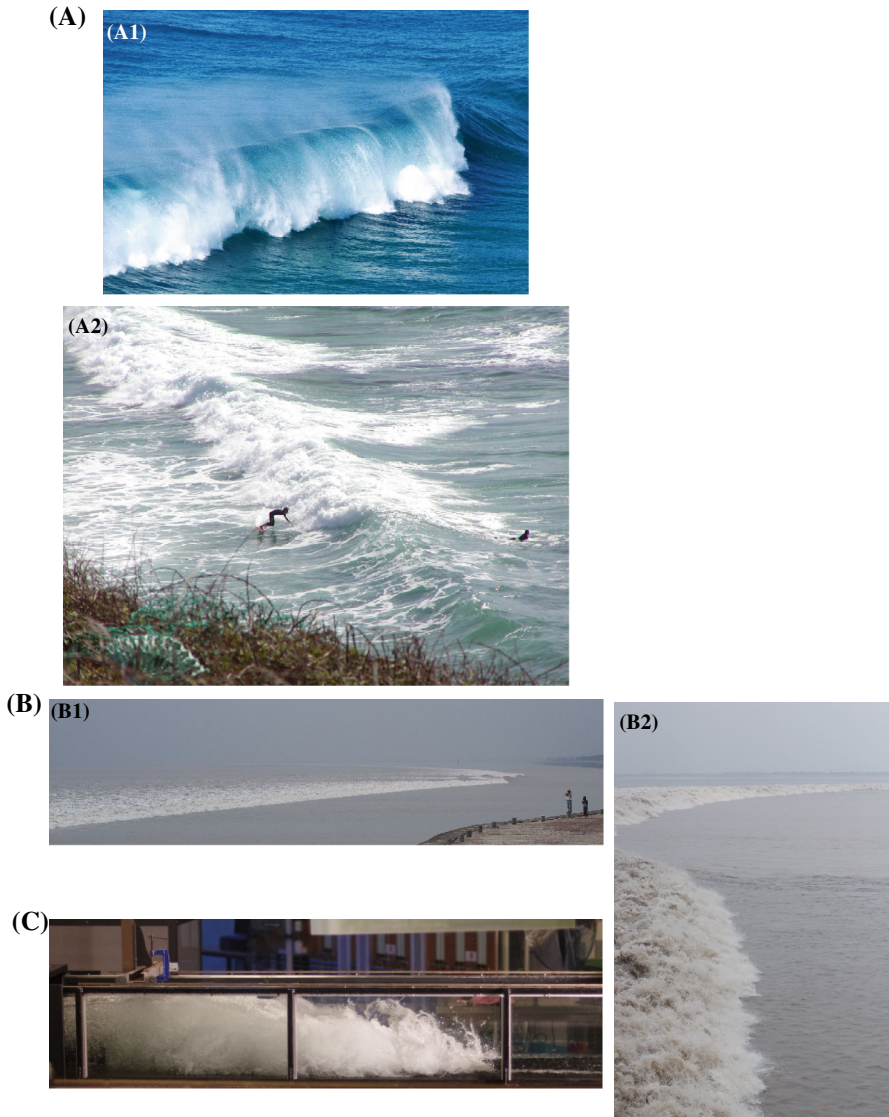


Fig. 2 Air entrainment in breaking waves, bores and jumps. **a** Breaking waves. *a1* Plunging breaking off Main Beach, North Stradbroke Island (Australia) on 19 April 2014—Shutter speed: 1/400 s, *a2* spilling breaker off Pointe du Grand Minou (Brest, France) on 18 March 2004—Shutter speed: 1/800 s. **b** Breaking tidal bore of the Qiantang River (China) on 11 October 2014. *b1* Bore approaching the old seawall at Xinchang at 12:50, *b2* Bore roller propagating (from left to right) parallel to the seawall at Qilimiao at 13:20—The roller height was about 2.5 to 3 m, the bore celerity 4 to 5 m/s and $Fr \sim 2$ —Shutter speed: 1/6400 s. **c** Hydraulic jump roller (steady flow direction from right to left): $Fr = 7.5$, $Re = 1.4 \times 10^5$, $d_1 = 0.03$ m, shutter speed: 1/1000 s

modified by the air entrainment, and the sound generated by the bubble clouds render the ships subject to detection. In hydraulic engineering, large spillways are often protected from cavitation damage by controlling aeration [76, 159].

Many numerical models (e.g. Boussinesq equations) used to study waves in the surf zone do not implicitly simulate the breaking process of the waves [54]. The wave-breaking effects have to be parameterised by incorporating additional terms in the mass and momentum equations (e.g. [13, 55, 100, 141, 171]). The challenge is to take the breaking process into account to ensure an accurate description of the surf zone, including the wave height decay and the setup development. The main consideration is to dissipate energy when wave breaking is likely to occur. Svendsen [167, 168] proposed the roller concept, in the form of a volume of water carried shoreward with the wave. Local roller thickness and mean front slope of the breaker were used to quantify part of the local momentum deficit. But the vertical surface roller of the breaking wave is only considered to play an important part in the momentum and energy conservation. However, the energy flux and dissipation during wave breaking remain difficult to quantify. Most recent modelling attempts are still struggling with the lack of physical knowledge of the finest details of the breaking processes, which makes the task of parameterising breaking effects very difficult since no universal scaling laws for physical variables have been proposed so far. Physical parameters, such as the height and length of the roller, have to be quantified and criteria have to be defined with critical bounded values to estimate where the waves break and stop breaking. Thus models still need calibration and further improvements [22].

The turbulent flow dynamics in bubble clouds is a very challenging numerical problem. Esmaeeli and Tryggvason [75] studied direct numerical simulations of buoyant bubbles in a two-dimensional periodic domain. They simulated 144 and 324 bubbles, showing that the work done by the buoyant bubbles increased the energy of flow structures much larger than the bubbles. But 3D direct modeling of air bubble entrainment and evolution at the scale of the surf zone is computationally unaffordable. Another way of tackling dispersed two-phase flows is using a continuum-mechanical approach [71]. Two-fluid models are used to model the polydisperse two-fluid bubbly flow based on mixture theory [26, 68, 127, 134, 162]. A first attempt to use a continuum type model for studying bubbly flow under surface breaking waves was made by Shi et al. [162]. They proposed a physically-based numerical model for prediction of air bubble population in a surf zone-scale domain. The air entrainment was formulated by connecting the shear production at air–water interface and the bubble number density with the bubble size spectra as observed by Deane and Stokes [67]. The model was initially fed with the entrained bubbles and used to simulate the evolution of the bubble plumes. This approach requires much less spatial and temporal resolution than needed to capture detailed air entrainment process in DNS simulations. The model results revealed that bubbles larger than 1 mm provide a major contribution to void fraction, while smaller bubbles contribute significantly to the cumulative interfacial area of the bubble cloud but do not contribute much to the total volume of air. Discrepancies between observations and model behaviour were nevertheless reported. Based on the works of Ma et al. [127], Derakhti and Kirby [68] used an Eulerian–Eulerian polydisperse two-fluid model in an LES framework. Detailed overviews on methods and models for CFD of multiphase flows can be found in textbooks [61, 72]. More information about turbulence modelling in the framework of multiphase flows is given by Labourasse et al. [107] and Bombardelli [17]. Smoothed-particle hydrodynamics (SPH) is also a mesh-free method which can be used to describe accurately the 3D surf zone hydrodynamics, as recently shown by Farahani and Dalrymple [77] who investigated some novel coherent turbulent vortical structures under broken solitary waves. The state-of-the-art is detailed by Gomez-Gesteira et al. [84] and Violeau and Rogers [177], who detailed a number of examples in which SPH simulations have been successfully used in fluid flow research and hydraulic engineering.

Numerical models still rely on experimental data. Detailed information on the temporal and spatial variations of the void fraction fields beneath breaking waves is required. Instantaneous void fraction and interfacial velocity data are critically needed to calibrate and improve numerical models of the two-phase flow generated beneath plunging and spilling breaking waves. Models for air-entrainment are critically dependent upon accurate estimates of the surface area affected by wave breaking. Controlled laboratory experiments and accurate measurements of void fraction and bubble size distributions beneath plunging and spilling breakers are still very challenging. When a wave breaks, the tip forms a liquid jet which impinges on the front face of the wave and creates an air cavity which breaks into bubbles. The characterisation of the bubble sizes resulting from the cavity collapse has to be measured and the trajectories of these entrained bubbles are also critical information. The initial stages of the breaking of a wave generated a large amount of bubbles production and to the distribution at greater depths. The bubble clouds will then form, grow and decay during the propagation of the turbulent air/water mixing region forming the bore, the temporal variations of all bubble cloud dimensions reflecting this evolution. The large volumes of air in bubbles rapidly evolve into a distribution of bubble sizes which interacts with liquid turbulence and organised motions.

The motion of bubbles relative to the liquid causes velocity fluctuations in the water column and increases the energy of liquid motion at the scales comparable with the bubble diameter [68]. Bubble plume kinematics and dynamics, and the structure of the turbulent bubbly flow under breaking waves constitute critical information to be taken into account for an accurate description of the wave breaking process [129]. While the former can be studied experimentally, the liquid–bubble interactions, i.e. the effects of dispersed bubbles on organised and turbulent motions, are still poorly understood.

When looking at a bore, whereas it has been generated by a stationary hydraulic jump, a surface wave breaking on the ocean or in the surf zone, or a tidal bore propagating upstream a river, the question is: are we looking at the same flow? Is there only one bore structure, or are there variations depending on the initial conditions leading to its occurrence and behaviour? To what extent can we compare the bores and use the quantities through similarity? It is the aim of this contribution to contribute to the transfer of knowledge from detailed measurements realised in hydraulic jumps and tidal bores, to the wave breaking investigation. The first part of the article is dedicated to the identification of the knowledge gaps encountered when attempting to simulate numerically the hydrodynamics of breaking waves and a review of the various analogies which have been proposed in the literature. The next part reports on the state-of-the-art of the studies focusing on the void fraction and velocity analysis under breaking waves, tidal bores and hydraulic jumps. Based on this survey, we attempt to identify and assess the quantities which can be considered for possible analogies. The most recent data are revisited and scrutinised for the use of most advanced numerical models to educe the surf zone hydrodynamics, highly influenced by the wave breaking process. An open discussion is proposed to explore the actual practises and propose perspectives based on the most appropriate analogy, namely the tidal bore.

2 Knowledge gaps for the modelling of the surf zone hydrodynamics

2.1 Current state of practice in numerical modelling and limitations

Most numerical models only consider macro-scale roller properties. The roller formation and propagation have been shown to be a highly unsteady process, with air entrainment and turbulence generation. The most advanced models, which are generally used to simulate non-linear wave transformations in coastal areas, are based either on the non-linear shallow water equations (NSW), the Boussinesq-type equations (BT), or some form of hybrid model. Extensive developments and break-through progress have been made recently for a large variety of coastal engineering applications (e.g. [3, 22, 100, 171]). A key feature, the breaking process, is however not explicitly simulated and missing in these models. Several approaches and parametrisations have thus been proposed to introduce wave breaking in NSW and BT models. Any such approach requires the quantification of energy dissipation, dynamically activated when wave breaking is likely to occur. Some physically based criteria have to be able to activate or deactivate these extra terms and simple expressions are generally favoured. Simple quantities include geometrical aspects of the roller, including heights, lengths and angles, easily extracted from any visual observations in laboratory and in the field. All these quantities cannot be estimated from a single experiment. Instead a composite set of data and practices have been elaborated though time by looking at various analogue flows, and some variations have been proposed in order to fill the gaps.

Practically, most numerical models need to evaluate:

1. A Froude number Fr characteristic of wave breaking, of when it occurs and stops (with Fr varying with water depth). Currently, an accepted value for the transition between non breaking and breaking waves has been identified in Froude number range between 1.3 and 1.6 [145]. This is based upon the analogy with non-breaking undular hydraulic jump and bore [46, 78, 104, 117, 173];
2. The roller height h_r , derived from momentum considerations (see Appendix 2);
3. The roller length L_r , determined empirically. A common parameterisation is $L_r = 2.91 \times h_r$ [87], although the re-analysis of large-scale experiments suggests $L_r/h_r \approx 1$ to 8 (Fig. 5). In Fig. 5, steady breaker, stationary hydraulic jump and tidal bore data are compared;
4. The mean front slope angle ϕ [161], typically between 8° and 30° for the termination and initiation of the breaking event respectively;
5. The roller celerity (or celerity of the breaking wave);
6. The energy dissipation in the roller region;
7. The bubble size distributions, often improperly estimated based upon Hinze's [89] model developed in the case of a single droplet under non-coalescing conditions (!).

To estimate most of these quantities, flow analogies have been considered, but some limitations are clearly identified and some modifications, based on new experimental data analysis, are proposed in the following sections.

2.2 Flow analogies or not?

A number of analogies were proposed between breaking waves, bores and jumps (Appendix 1). Appendix 1 lists a number of early seminal references and Fig. 1 presents

definition sketches. The steady breaker configuration was proposed as a simplification of the spilling breaker [6, 7]. Important results were obtained [8, 59, 63, 73, 121], but there is still on-going argument about the validity of this analogy [102]. Further links were developed between breaking waves and steady flow configurations. These encompassed comparisons between plunging breakers and plunging jets [44, 47, 48, 56, 93, 143, 160], between spilling breakers and stationary hydraulic jumps [23, 24, 123, 128, 147] and between spilling breakers and translating hydraulic jumps (also called positive surges or tidal bores) [24, 123, 147]. In parallel, there have been numerous discussions about the similarities and differences between stationary and translating hydraulic jumps (e.g. [65, 118, 164, 174]), although the open channel hydraulic literature develops the same integral approach for both types [32, 41, 88, 118].

To date, the mechanistic connections between these flows are not well understood and have not always been successful. Wave-plunging jet conditions appear to produce a qualitatively different type of impact, with almost no penetration into the oncoming flow and a pronounced splash that cascades multiple times down the face of the wave. What is better characterised however, is the volume of air trapped by the initial contact of the jet with the wave face, which has been numerically simulated, and its shape has been successfully modelled, at least for a limited set of conditions (e.g. [126]). However, the processes that follow the initial contact are only known qualitatively for the majority of the breaking conditions, and thus still require further study in order to acquire improved physical understanding. Furthermore, wave breaking is a combination of transient processes which evolve within the breaking duration making adequate physical understanding a challenging proposition. Overall, “*In studying any turbulent flow it is very helpful if it can be shown to be similar to other well known flows*” [147]. Below, a number of seminal flow configurations are explored and the relevance of flow comparisons is discussed.

3 Void fraction kinematics

3.1 Breaking waves

Führboter [79] discussed the correlation between the turbulence generated in the surf zone and the amount of air entrained during the breaking of the waves, as well as the sudden reduction of wave height and energy. He highlighted the importance to study quantitatively the air entrainment process for a detailed comprehension of the surf zone physics. Vagle and Farmer [175] and recently Anguelova and Huq [1] reviewed the different techniques used to quantify the void fraction under breaking waves. Both works concluded that combined techniques were the best approach. Indeed, the higher the concentrations of bubbles within bubble clouds, the more difficult it is to count and measure individual bubbles.

Some studies have been conducted in field while others have been completed in physical wave tanks. Thorpe [170] studied wind-waves breaking and speculated that wind speed, salinity, and temperature were major factors, possibly responsible for existing discrepancies that arise when comparing data from different sources. Monahan [133] proposed the terms Alpha-plume (high void fraction, short lifespan), Beta-plume, and Gamma-plume (low void fraction, long lifespan) to describe the evolution of a bubble cloud, from its formation to its disappearance (e.g. dissolution, degassing and advection). Most field studies confirmed that the Alpha-plumes consist of high void fractions (10 % or more) with

large bubble sizes (radii ranging from tens of micrometers to millimeters). At the other end of the process, the Gamma-plume were observed to be very low void fraction between 10^{-5} and 10^{-8} and containing bubbles with radii on the order of $O(10\text{--}100)$ μm . The lifetime of a whole bubble cloud may be about a hundred of seconds. The bubble clouds are also generally confined to the first few meters of the water column. For example, Lamarre and Melville [110] compared field and laboratory void fraction measurements obtained with an impedance probe, and showed large void fraction values at shallow locations while lower void fraction values were found deeper. Deane [66] used acoustic and optical measurements of individual breaking waves in the surf zone, off La Jolla Shores beach, California. Total void fractions of 0.3–0.4 were measured, consisting of bubbles with radius greater than 1 mm. Stokes and Dean [165] observed that the time scale for the generation of clouds of submillimetric bubbles was on the order of about 90 ms. Dahl and Jessup [64] found comparable quantities in deep-ocean studies. Gemmrich and Farmer [83] measured void fraction values (e.g. 10^{-2} at 0.25 m below the free-surface), associated with low penetrating breaking events (spilling breakers), while they speculated that higher values of void fractions found deeper would be associated with more energetic violent events (plunging breakers). Interestingly Gemmrich [82] found higher turbulence levels within the wave crest region of the breaking waves, suggesting that the bubble fragmentation process is mainly driven by turbulence. Most studies reported that void fraction changes significantly during the lifetime of the bubble cloud, from high void fractions in the first seconds of the breaking event to residual void fractions persisting for long times. Most field studies consisted in wind-waves breaking observations, with only few events giving data susceptible to be accurately analysed.

A lot of studies investigated the hydrodynamics in the surf zone, especially the general mechanisms involved during the breaking process [146], the generation of turbulence [10], and sediment transport. When waves break, the flow suddenly exhibits a violent transition from irrotational to rotational motion over the entire water column. Two main types of breaker types have been studied: (1) the spilling breakers, where white foam, consisting of a turbulent air/water mixture, appears at the wave crest and spills down the front face of the propagating wave; and (2) the plunging breakers, where the front face of the steepening wave overturns and impacts the forward face of the wave. These two breaker types have been shown to have similar initial motions, but with different length scales [9]. When approaching a beach, the waves change form due to the decrease in water depth. The forward face of the wave steepens and the wave becomes asymmetric. Once the front face becomes almost vertical, a jet of liquid is projected from the crest of the wave. The tongue of water thrown from the crest develops and free falls down forward into a characteristic overturning motion, and eventually hits the water at the plunge point. Depending on the position of the plunge point, different breaker types can be observed. If the plunge point is located very near to the crest of the wave, the resulting splash is directed down the wave leading to a spilling breaker. Otherwise, if the jet is ejected farther towards the lower part of the face of the steepening wave, the wave becomes a plunging breaker. The plunging jet encloses an air pocket when it finally hits the wave face at the plunge point. The jet re-enters the water after impact, forcing up a second jet, called splash-up. The early works of Miller [132], Basco [9], Jansen [97] and Bonmarin [18] were dedicated to qualitative description of the dynamics of the breaking process, the air entrainment and the evolution of the large-scale geometric properties of bubble plumes. The overturning process, subsequent overturning motion and plunging jet impact were described, resulting in the identification and tracking of breaker vortices trajectories. Some information about the evolution (size, shape and position) of the bubble plumes were also detailed. The jet-splash

cycles, occurring several times in a single breaker, have been shown to be responsible for the generation of a sequence of large-scale vortices with a horizontal axis of rotation, some of these eddies have been shown to be co-rotating vortices and some counter-rotating vortices depending on the splash-up mechanism [18, 132]. Nadaoka et al. [142] detailed the flow field under a turbulent bore propagating towards the shoreline, resulting from a spilling breaking wave. Large-scale horizontal eddies are present in the bore front, while behind the wave crest the flow structure changes rapidly into obliquely downward stretched three-dimensional (3D) eddies, so-called ‘obliquely descending eddies’. Lin and Hwung [120], Govender et al. [85] and Kimmoun and Branger [101] also described the large motions of aerated regions under plunging breaking waves, with splash-ups and vortical structures.

Miller [132] measured the average bubble concentration in plunging and spilling breakers and indicated a larger bubble density presence in plunging breakers (about 31 % in the late stage compared to 19 % for spilling breakers); these results were in agreement with earlier descriptions from Miller [131]. Lamarre and Melville [109] concluded that a large portion of the mechanical energy of the wave was lost in entraining the bubble clouds. High values of void fractions (up to 100 %) were found next to the free-surface, and void fractions of at least 20 % were observed for up to half a wave period after the breaking occurrence. They later confirmed that air entrainment was closely related with the energy dissipation of the breaking wave [111]. Several other works provided more comprehensive laboratory measurements of the void fraction in breaking waves, detailing the vertical and horizontal distributions of void fraction. Cox and Shin [60] measured the void fraction in the aerated region at a point using a capacitance probe, and observed peak ensemble-averaged void fractions in the range of 15–20 %. Surprisingly, they measured higher void fractions under the spilling breakers than under the plunging breakers. The temporal variation of void fraction, above and below the still water level, was analysed using three breaker types (spilling, spilling/plunging and plunging). The temporal variation of void fraction above the still water normalized by the wave period and average void fraction appears to be remarkably self-similar (independently of the breaker type). Hwung et al. [94] found a deeper penetration of air bubbles under plunging breaking waves and higher void fractions (18 %), compared to the spilling breaking waves (12 %). Similarly Hoque and Aoki [90], using a conductivity probe, measured maximum void fractions of 20 and 16 % beneath plunging and spilling breakers, respectively. Mori et al. [135] obtained void fractions of 19 % beneath spilling breaking waves and 24 % beneath plunging breaking waves, using dual-tip resistivity void probe. Interestingly they also studied scale effects according to Froude similarity and using two different scaled experiments. Void fractions were affected by the geometric scale, with larger quantities being found in the larger experiment, while the bubble size spectra proved to be nearly independent. Kimmoun and Branger [101] estimated the evolution of void fractions using particle image velocimetry images and velocity measurements. They reported large void fractions of up to 88 % in the first splash-up location, decreasing slowly when the breaking wave propagates towards the shore, with values between 20 and 30 %. Much lower void fractions were found in other studies. Kalvoda et al. [98] investigated the geometric and kinematic characteristics of large air bubbles clouds produced by spilling breaking wind waves. They observed that the lifetime of the bubble cloud was about 1.4 times the wave period, with bubbles diameters in the range of 1.0–10 mm. They found a void fraction of about 0.4 %. Leifer et al. [113] reported void fractions between 0.2 and 2.3 % beneath breaking wind waves, using a video system to characterise the bubble clouds. Blenkinsopp and Chaplin [14] studied plunging, spilling/plunging and spilling breaking waves. They calculated

integral properties of the bubble clouds and splash-ups, such as areas and volumes of air entrained, trajectories of centroids and energy dissipation, and showed remarkable similarity between plunging and spilling breakers. Their data indicated that the evolution of the bubble clouds was subjected to scale effect. Rojas and Loewen [156] detailed the void fraction evolution in spilling and breaking breakers. They observed that beneath plunging breaking breakers, the mean void fraction ranged between 1.2 and 37 %, while beneath spilling breaking waves, the mean void fraction ranged between 17 and 29 %. They found that “*an energetic spilling breaker may entrain approximately the same volume of air as a steeper, larger-amplitude plunging breaker*”. They identified and tracked successive bubble clouds, detailed the void fractions at each step of the breaking events, and found that, beneath the spilling breaker, the celerity of the bubble cloud compared with the phase speed. Beneath the plunging breaker, the celerity of the air cavity was about 70 % of the phase speed. This has to be compared to the celerity of the bubble cloud entrained by the propagating splash-up which has been measured to be about 90 % of the phase speed. Blenkinsopp and Chaplin [14] and Rojas and Loewen [156] found that the volume of air entrained by the splash-up, observed during a plunging breaking event, was greater than the volume of air entrained by the initial plunging jet (about 60 % more). More recently Anguelova and Huq [1] used an imaging technique to quantify the phase dependent void fraction, and measured values reaching 80–99 % at the wave crest phase and decreasing to 20–30 % at the trough phase. Lim et al. [119] confirmed these results in the case of a plunging breaker. They showed that the distribution of the turbulent intensities matched the vorticity and void fraction fields. Nevertheless, some differences could be observed in the experimental results for the peak values of void fraction, indicating a strong temporal and spatial variability in the unsteady breaking waves [119]. The difference in the locations of the measurements and the method used to generate the breaking could also be responsible for the discrepancies. Some authors indicated that the mean void fraction could be modelled by a linear function of time followed by an exponential decay. Hoque and Aoki [90] found that the void fraction distribution followed the analytical solution of an advection equation. This is not surprising as there is a general consensus about in void fractions contours in the breaking waves, shapes and general kinematics of the aerated regions. However, some differences can also be noted. Lamarre and Melville [109] found that that the temporal variation of the normalized void fraction in deep water breakers could be fitted by a power law $t^{-2.3}$, while Rojas and Loewen [156] found the decay of void fraction followed a power law $t^{-2.6}$. Lim et al. [119] reported similar findings. Cox and Shin [60] found a linear growth followed by exponential decay, but with a different rate, which could be attributed to the shallow-water conditions used in their works.

3.2 Tidal bores

Undular tidal bores are observed for Froude numbers less than 1.3–1.4, and breaking tidal bores with a marked roller are seen for Froude numbers large than 1.4–1.6 [37, 104]. Velocity measurements in breaking tidal bores were performed using particle image velocimetry and acoustic Doppler velocimetry with most data obtained in the clear-water column below the aerated roller region and for Froude numbers less than 2.5 [38, 69, 91, 105]. The data indicated a sharp deceleration of the flow associated with the bore passage, as well as large fluctuations of all velocity components during and shortly after the bore roller passage [105, 114].

Air–water flow measurements in tidal bores are rare. Leng and Chanson [114] highlighted some distinctive air bubble entrainment at the toe of the roller. Their data showed a

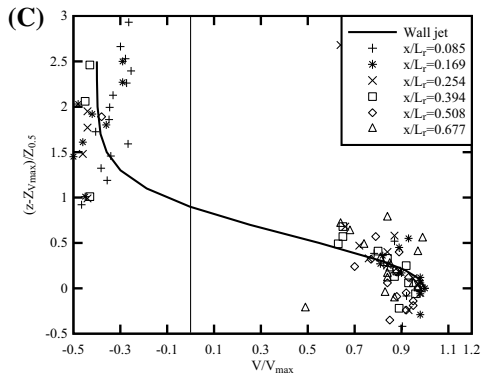
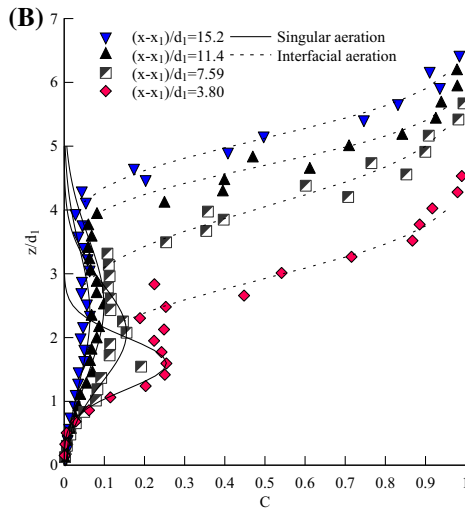
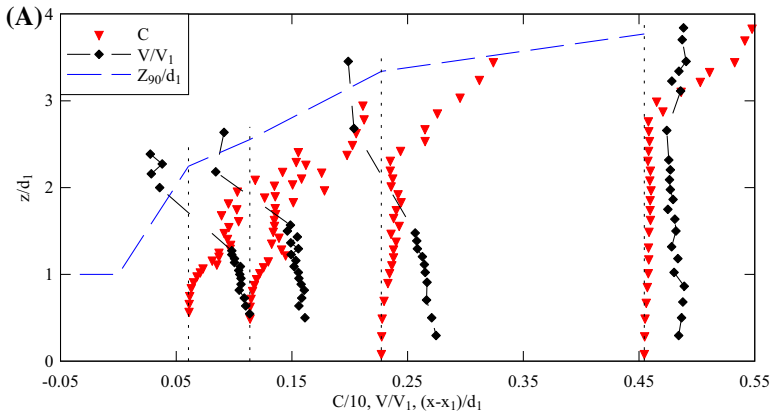
substantial number of bubbles with millimetre sizes: i.e., between 1 and 5 mm, with larger bubbles detected at higher vertical elevations in a more intermittent manner. The same data set showed that the toe perimeter shape fluctuated rapidly with transverse distance and time, and large fluctuations in bore celerity were observed. That is, the celerity of the roller toe fluctuated rapidly with both time and transverse distance, although in a quasi-two-dimensional manner on average [115]. Yet both laboratory and field observations hinted to the existence of large-scale three-dimensional bubbly structures [43, 114, 116].

3.3 Hydraulic jumps

A hydraulic jump is the sudden and rapid transition from a supercritical to subcritical flow, characterised by the development of large-scale turbulence, surface waves and spray, energy dissipation and air entrainment (Figs. 1, 2). Undular hydraulic jumps, observed for Froude numbers less than 2–3, are not discussed herein. The breaking jump is a turbulent shear flow [92, 150, 157], and vorticity is advected in the air–water shear zone. The first successful air–water flow measurements were conducted by Rajaratnam [149]. Using hot film anemometry, Resch and Leutheusser [153] and Babb and Aus [2] measured distributions of Reynolds stresses and turbulence intensity in hydraulic jump rollers. High-quality data were obtained using dual-tip phase-detection probes, allowing significant improvements on the characterisation of the air–water flow field inside the jump roller. Most studies were conducted for inflow Froude numbers greater than 5 [39, 49, 178]. Relatively Fewer studies investigated hydraulic jumps with lower Froude numbers [29, 140]. Other research works also used flow visualization techniques [112, 137].

All experimental investigations in breaking jumps showed some intense air entrainment, with singular air entrainment at the roller toe and interfacial aeration across the roller free-surface [178]. Air is entrapped at the discontinuity between the impinging flow and the roller: i.e., the roller toe (Figs. 1, 2). The roller toe perimeter is a line source of air bubbles, as well as a line source of vorticity [31, 91]. In the shear region downstream of the roller toe, the local maximum in void fraction C_{\max} decays longitudinally in a quasi-exponential manner [49, 140]. A key feature is the developing shear layer and the recirculation region above. The turbulent shear flow is somehow analogous to a wall jet although basic differences between ideal wall jet and hydraulic jumps include the effect of longitudinal pressure gradient $\partial P/\partial x < 0$, conservation of mass, and the natural forcing which is likely to enhance the two-dimensionality and periodicity of coherent structures [99]. In the jump, the maximum velocity V_{\max} decays longitudinally as $x^{-1/2}$ [39, 49, 139].

Figure 3 presents some typical air–water flow measurements in hydraulic jumps with breaking roller. Figure 3a shows longitudinal variations in vertical distributions of void fraction and interfacial velocity in the roller, where C is the time-averaged void fraction, V is the interfacial velocity, x is the longitudinal distance from the roller toe, L_r is the roller length, z is the vertical elevation, and d_1 and V_1 are the inflow depth and velocity respectively. Overall the measurements highlighted two distinct air–water flow regions: (1) the air–water shear layer, and (2) the upper free-surface region above. The shear layer is characterised by strong interactions between the entrained air bubbles and turbulent coherent structures, associated with a local maximum in void fraction, bubble count rate and longitudinal velocity. In the shear layer, the distributions of void fractions follow an analytical solution of the advection–diffusion equation for air bubbles assuming singular air entrainment at the roller toe:



◀ **Fig. 3** Air bubble entrainment in a hydraulic jump with a marked roller. **a** Longitudinal variations of vertical distributions of void fraction and interfacial velocity—Data set: Chachereau and Chanson [29], $d_1 = 0.044$ m, $Fr = 3.1$, $Re = 8.9 \times 10^4$. **b** Vertical distributions of void fraction—Data set: Chachereau and Chanson [29], $d_1 = 0.0395$ m, $Fr = 5.1$, $Re = 1.3 \times 10^5$. **c** Vertical distributions of interfacial velocity in the roller—Data set: Chanson [37], $d_1 = 0.018$ m, $Fr = 9.2$, $Re = 6.9 \times 10^4$

$$C = \frac{\frac{q_{air}}{q}}{\sqrt{4 \times \pi \times D \times x'}} \times \left(\exp\left(-\frac{(z'-1)^2}{4 \times D}\right) + \exp\left(-\frac{(z'+1)^2}{4 \times D}\right) \right) \tag{1}$$

where $x' = x/d_1$, $z' = z/d_1$, D is a dimensionless diffusion coefficient, $q = V_1 \times d_1$, and q_{air} is the entrained air flow rate per unit width. D and q_{air}/q are derived from best data fit. In the upper free-surface region above, the void fraction increases monotonically with increasing distance from the bed from a local minimum up to unity, following an analytical solution of the advection–diffusion equation for interfacial aeration/de-aeration:

$$C = \frac{1}{2} \times \left(1 - \operatorname{erf}\left(\frac{1}{2} \times \sqrt{\frac{V_1 \times x}{D_t}} \times \frac{z - Z_{50}}{x}\right) \right) \tag{2}$$

where D_t is a diffusion coefficient, Z_{50} is the elevation where $C = 0.5$ and erf is the Error function. Both Eqs. (1) and (2) are compared with experimental data in Fig. 3b, with solid lines and dashed lines respectively. The interfacial velocity distribution presents a self-similar profile close to that of wall jet:

$$\frac{V - V_{recirc}}{V_{max} - V_{recirc}} = \exp\left(-0.88 \times \left(\frac{z - z_{Vmax}}{z_{0.5}}\right)^2\right) z_{Vmax} < z \tag{3}$$

where V_{max} is the maximum velocity in the shear region, V_{recirc} is the negative recirculation velocity, $z_{0.5}$ is the elevation where $V = (V_{max} + V_{recirc})/2$ and z_{Vmax} is the elevation where $V = V_{max}$. Equation (3) is compared with experimental data in Fig. 3c. Note the negative time-averaged recirculation velocity, with $V_{recirc}/V_{max} \sim -0.4$ to -0.6 on average [39, 185] (Fig. 3c). Further observations include the integral turbulent length scale L_t characterising the size of large turbulent eddies advecting the bubbles in the hydraulic jump roller [34, 179]. Typical results highlight the relationship between integral turbulent length scale and inflow depth, with on average $L_t/d_1 \sim 0.5$. Moreover, several studies were dedicated to the analysis of the clustering process in a hydraulic jump [86], focussed on the interaction between air bubbles and turbulence, and confirming the influence of the bubble clustering on the surrounding flow field whereby hydrodynamic interactions and enhanced velocity fluctuations can play an important role.

4 Discussion

Based on the previous section, we propose a discussion on limitations, disagreements and obstacles which have to be overcome to improve the knowledge of the turbulent air–water dynamics encountered in breaking waves and bores. We focus on the flow aeration and bubble sizes distribution in the water column, water salinity and the definition of the Froude number.

4.1 Flow aeration and bubble sizes

Very few detailed studies on air entrainment induced by breaking waves exist (Sect. 3.1). A number of issues remain and definitive conclusions have not yet been drawn. Wave conditions and characteristics are not easily comparable. For example, some studies were centred on deep-water breaking waves while others focused on depth-limited conditions, some breaking waves were mechanically generated, others were wind-waves. Further the metrology (optical, acoustic, laser, conductivity BIV, PIV, video, photographs) and experimental apparatus (single or double probes, measurements locations, assumptions for analysis, mixture density estimations for wave characteristics, etc.) often suffered from limitations and inaccuracies (e.g. [27, 33, 60]). Phase-detection needle probes are intrusive point measurements, while BIV or PIV are non-intrusive but remain inaccurate when operated in highly aerated turbulent flows (bubble clustering, shape changes, light reflection, image processing technique and analysis). Sampling rate is another issue when trying to characterise turbulent bubbly flow properties. A number of studies thus used combined techniques to ensure a certain level of confidence in their measurements.

Several findings may be highlighted. All authors reported that the energy of the waves was dissipated during the early stages of the breaking events, due to the splash-up kinematics, turbulence generation and air entrainment process. The kinetic energy was found to decay as t^{-1} , both experimentally [70, 109, 110, 130, 152] and numerically [52, 95, 96, 108, 125, 126]. The same decay rate was observed for all breaker types (spilling, weak plunging and plunging) [126, 130], while similar integral properties in terms void fraction were comparable for different types of breaking waves [14, 60]. Locations of air entrainment in the roller can be identified at the toe of the advancing roller, and on the whole interface of the roller, where multiple splashes are observed [18, 119, 120, 132, 142, 156]. Large coherent eddies play a significant role in turbulent production due to the large velocity gradients and contribute to shear in the mean flow and fluctuations.

The highest velocities and turbulence intensities are found in the front part of the wave crest, at the toe of the wave roller and in the shear regions. In both spilling and plunging waves, the propagation of the roller to the shore line is associated with higher levels of turbulence [85]. The breaking bore is widely recognized as being the primary source of turbulence under breaking waves. The void fraction appeared to be correlated with the flow turbulence and turbulent kinetic energy [60, 135], but experimental results have not yet proved that the turbulent properties are enhanced by high concentrations of bubbles, and vice and versa. Indeed, the relations between void fraction and bubble size distributions, and between void fraction and turbulence, remain unclear: “*the entrained bulk of air and bubbles generate turbulence which breaks coarser bubbles into finer ones in this phase*” [136]. Gemmrich [82] speculated that the bubble fragmentation process is mainly driven by turbulence. But the bubble dynamics might also be a major source of turbulence in the surrounding fluid.

Altogether breaking waves can produce large millimetre bubbles, although smaller bubbles may be found in the breaking region (Table 1). Table 1 summarises a few detailed observations. Larger bubbles are mainly present in the roller region, while much smaller bubbles with large residence times may be found deeper. Bubble populations under breaking waves are very inhomogeneous in time and space. Bubbles can be observed to split under several breakup mechanisms, including turbulent induced breakup, shear-driven breakup resonant oscillation and tip-streaming [35, 57, 169]. The dynamics of a bubble

Table 1 Summary of bubble size observations

Flow topology	Description	Equivalent bubble radius (mm)	Reference
Breaking waves	Open ocean (Fig. 14)	0.8–1	Bowyer [20]
	Open ocean (Fig. 6)	1	Dean and Stokes [67]
	Laboratory focused waves paddle (10 cm plunging) (Fig. 4)		
	Open ocean	0.7	Stokes et al. [166]
	Laboratory	1–1.7	Leifer et al. [113]
	Wind + paddle (~12 cm breaking height)		
	Fresh (but not clean) water		
	Laboratory focused waves paddle (~20 cm plunging)	1.5	Rojas and Loewen [156]
	Fresh water		
Plunging jet	Laboratory wave paddle sloping beach spilling—plunging (12.6–16.5 cm mid-scale/5.0–6.5 small-scale)	2.01 (mid-scale)—4.28 (small-scale)	Mori et al. [135]
	Laboratory wave paddle submerged reef spilling—plunging (9.5 cm)	1.7–2.4	Blenkinsopp and Chaplin [15]
	Tap water		
	Circular plunging jet ($\varnothing = 25, 12.5$ and 6.85 mm)	4.7 ($\varnothing = 25$ mm) 2.2–3.7 ($\varnothing = 12.5$ mm)	Chanson et al. [32]
	Tap water (Table 3)	1.7–2 ($\varnothing = 6.85$ mm)	
	Circular plunging jet ($\varnothing = 12.5$ mm)	2.2–3.1 (tap water)	Chanson et al. [48]
Tap water, saltwater, seawater (Table 5)	2.3–3.3 (saltwater) 1.5–2.3 (seawater)		

under unsteady perturbations is affected by the balance between forces acting on the bubble, but the residence time of the bubble in the turbulent flow field should also be taken into account [31, 81]. A large amount of bubbles are generated and broken in the shear zones, where velocity gradients play a great role in the breakup process. Current breakup models are unable to quantify accurately the breakup rate and bubble size distributions in a complete unsteady turbulent flow with high void fractions, partly because the two-phase flow mixture beneath breaking waves is a highly unsteady process, never reaching an equilibrium. As an illustration, Fig. 4 presents the normalized probability distribution functions of bubble radii beneath a plunging seawater jet, at three vertical elevations. In Fig. 4, each histogram column represents the probability of bubble radius in 0.25 mm increments: that is, the probability of a bubble radius from 1.0 to 1.25 mm is represented by the column labelled 1.0. The last column (i.e. 0.5) indicates the probability of bubble radii large than 5 mm. The data showed a broad spectrum of bubble sizes at all elevations, from less than 0.25 mm more than 5 mm (Fig. 4). The bubble radius distributions showed a preponderance of small bubble sizes relative to the mean: the mode was between 0 and 0.5 mm, although the mean radius was about 1.5–2.3 mm (Table 1). If equilibrium exists, the ‘equilibrium’ bubble size distribution is dictated by all the events taking place in the flow, in particular by the relative rates of bubble breakup and bubble coalescence, the bubble-turbulence interactions and the bubble clustering.

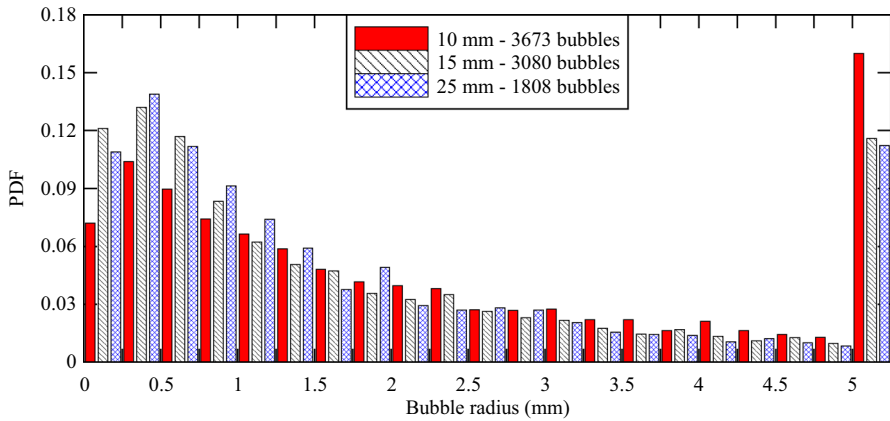


Fig. 4 Pseudo-bubble radius distributions in seawater generated by a vertical circular plunging jet, at 10, 15 and 25 mm beneath the free-surface—Data set: Chanson et al. [48], jet diameter: 12.5 mm, impact velocity: 3.1 m/s, water solution: Pacific Ocean seawater off Japan coastline—All bubble sizes were recorded in air–water regions with void fractions greater than 2 %

4.2 Water solution: freshwater, saltwater or seawater?

A number of studies tested the influence of salinity on the air bubble entrainment, although there is no agreement between most published results. A majority of such studies tested experimentally saltwater solutions, typically by gradually adding salt to freshwater: i.e., synthetic seawater [20, 28, 122, 160] (Also Table 1). Differences have been attributed to some form of inhibited coalescence process in saltwater. Controlled experiments with genuine seawater are rare (e.g. [16, 25, 48]). In strongly aerated regions (void fractions $>2\%$), the results showed differences between freshwater, saltwater (synthetic seawater) and genuine seawater in terms of void fraction and bubble sizes. Despite differences in trends, an overall conclusion was that large amount of air bubbles were entrained in all solutions, and the majority of bubbles in the aerated flow region had radii on the order of a millimetre (Fig. 4).

It must be stressed however that the rare data were obtained with different geometric scales. In air–water flows, experimental results demonstrated that scale effects may be significant [31, 42, 45, 151, 184], in particular in terms of bubble numbers and sizes. In turn, small scale experiments are more sensitive to changes in water salinity, and this may bias the findings.

4.3 Froude number and definition

The definition of the Froude number is of paramount importance, because it is used to detect the breaking event onset and termination during the evolution of the waves in the surf zone. It is also the critical parameter allowing scaling of the data, assuming analogies between hydraulic jumps, tidal bores and rollers due to breaking waves. Table 2 regroups a number of definitions. Several criteria have been used in the past to detect the inception of wave breaking. Wave steepness, based on Stokes' limiting wave height, has been widely used as an proxy for wave breaking. The occurrence of breaking has also been related to the energy content in the waves, to the acceleration of the free-surface, or to the

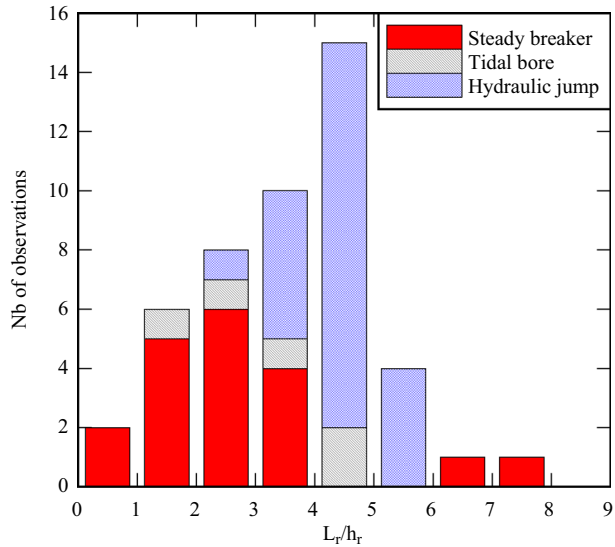
Table 2 Froude number definitions in breaking waves, bores, surges and jumps

Froude number definition	Reference	Quantities	Comment
$Fr = (U + V_1) / (g \times d_1)^{1/2}$	Bazin [11], Boussinesq [19]	Implies the knowledge of the current condition V_1 and d_1 flowing adversely the roller, together with the celerity of the roller toe U	Classical definition, satisfying the mass and momentum conservation equations, in a rectangular horizontal channel
$Fr = (U + V_1) / (g \times A_1/B_1)^{1/2}$	Chanson [41]	Implies further the knowledge of the initial cross-section area A_1 and free-surface width B_1	Application of mass and momentum conservation equations for an irregular-shaped channel
$Fr = (c_{crest} - u_{trough}) / c_{trough}$	Okamoto and Basco [145]	Velocity of the crest, trough and depth averaged velocity in the trough region	Can be applied to deep water breaking waves
$Fr = ((2 \times d_2 / d_1 + 1)^2 - 1/8)^{1/2}$	Tissier et al. [171]	Water heights upstream and downstream the jump	Not accurate enough [3]
$Fr = (1 + 3 / (2 \times H_r / d_1 + 1 / (2 \times (H_r / d_1)^2)^{1/2}))$	Tonelli and Petti [172]	Same as the previous definition, but written as a function of the roller height and water depth in front of the roller	Not accurate enough [3]
$Fr = u_s / c_b$	Bacigaluppi et al. [3] Cheng and Wang [53]	u_s is the free surface velocity at the crest of the wave, and c_b the wave celerity	Implies calibration. $Fr = 0.75$ to 1 found to be the value when waves start breaking [3, 53]. Problem: based on the idea that wave breaking occurs when the free surface velocity exceeds the wave celerity (which is not true for spilling, and true for the celerity inside the crest for plunging)

prescription of a limiting value to the fluid velocity at the crest of the wave prior to breaking (horizontal fluid velocity: [146] (see Fig. 2); [181]; vertical fluid velocity: [103]). However consensus and agreement has not been reached for the establishment of a simple, accurate and universal valid criterion. This is in part because wave breaking is a highly complicated process involving highly non-linear effects including varying bathymetries, currents, and wind (not taken into account in any study). An improvement in the quest has been the use of a Relative Trough Froude Number (RTFN, [145]), based on the analogy with a moving hydraulic jump in a one-dimensional open channel flow. The Froude number can be obtained, as detailed in Table 2, by the mean of the Π -theorem, momentum considerations (Appendix 2) and by simple construction considering the quantities available. A discussion is provided in Appendix 2, since consistency and physical adequacy are key features of this study. It is also important to consider the quantities available in the various sources of data (Table 2, third column) (Fig. 5).

The strength of a breaking roller and the rate of energy dissipation in the roller are directly linked to the Froude number [5, 21]. This is detailed in Appendix 2. The roller length L_r increases monotonically with increasing Froude number, as illustrated in Fig. 6a. For stationary hydraulic jumps, very detailed experimental measurements yielded:

Fig. 5 Probability distributions functions of roller aspect ratio L_r/h_r —Re-analysis of large-scale wave breaking experiments [58, 87], stationary hydraulic jump data [106, 138, 139, 178, 180], and tidal bore data [51, 138]



$$\frac{L_r}{d_1} = 6 \times (Fr - 1) \tag{4}$$

where d_1 is the upstream depth and $Fr = (U + V_1)/(g \times d_1)^{1/2}$ (see symbol definition in Fig. 1). Equation (4) is compared to stationary hydraulic jump and tidal bore data in Fig. 6a. Practically another relevant quantity is the length of the aerated region L_{air} . Typical experimental observations are reported in Fig. 6b, suggesting that the aeration region length may be about 1.5–2 times longer than the roller itself.

Another measure for the roller strength is the height of the roller h_r . Indeed the height of the roller increases with increasing Froude number. Basic momentum considerations show a unique relationship between roller height and Froude number for $Fr > 2$ (Appendix 2):

$$\frac{h_r}{d_1} = \frac{1}{2} \times \left(\sqrt{1 + 8 \times Fr^2} - 3 \right) \quad Fr > 2 \tag{5}$$

For $Fr < 2$, physical observations in tidal bores showed that the surface immediately upstream of the roller was curved upwards and the roller height was less than the difference in conjugate depths (Fig. 7). This is illustrated in Fig. 7, by comparing experimental data and Eq. (5). For breaking bore (i.e. $1.4 < Fr < 2$), the roller height data were best correlated by

$$\frac{h_r}{d_1} = 1.59 \times (Fr - 1.16)^{0.94} \quad 1.4 < Fr < 2 \tag{6}$$

The mean slope of the breaking roller can be obtained $\tan\phi = h_r/L_r$. When the height of the breaker h_r is lower than the difference in conjugate depths ($d_2 - d_1$), the front face of the breaking wave may not be fully saturated. Importantly the evolution of the roller is highly unsteady and depends on the evolution of many parameters, including the variation of the bathymetry or the current for example. Hence some simplistic parameters such as the roller height might not characterise accurately the breaking wave roller.

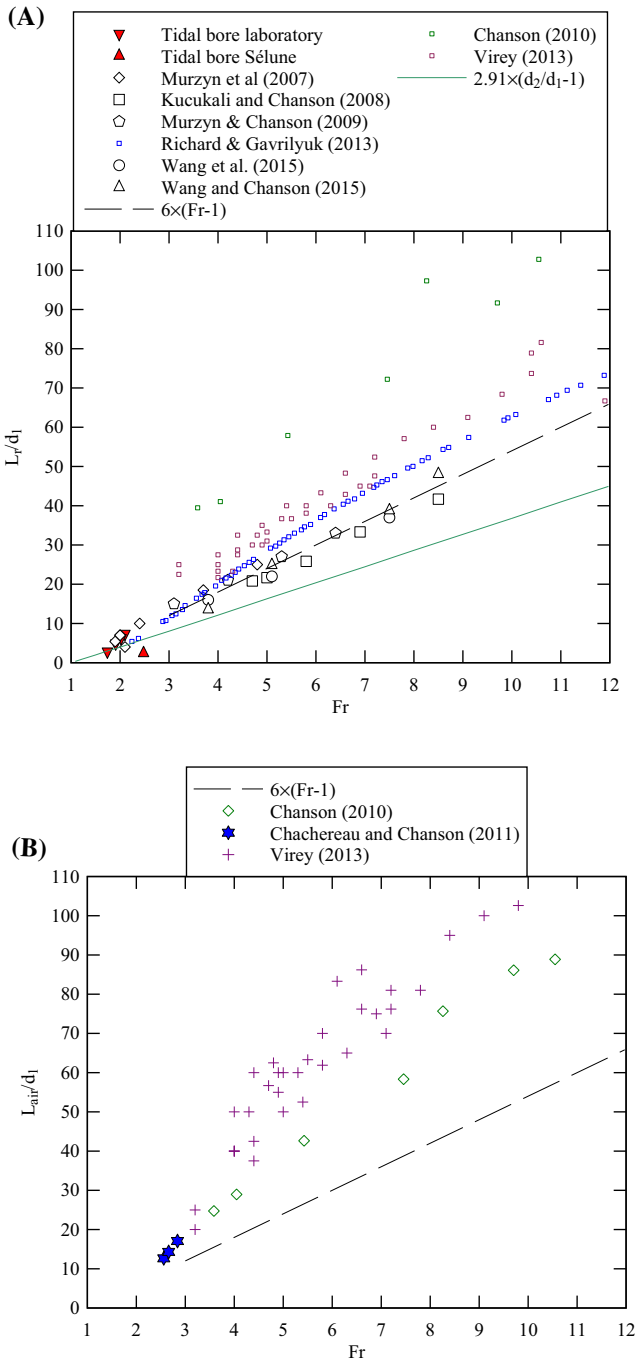
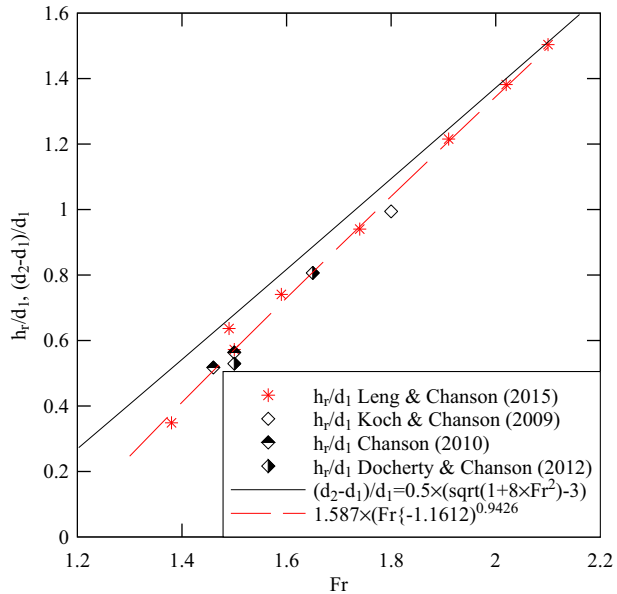


Fig. 6 Roller length and aeration length in breaking hydraulic jumps and tidal bores as functions of the Froude number ($Fr = (V_1 + U)/(g \times d_1)^{1/2}$). **a** Roller length in breaking hydraulic jumps and tidal bores—Most data are hydraulic jump data unless indicated in the legend; tidal bore data by Chanson and Toi [51]. **b** Aeration region length in hydraulic jumps

Fig. 7 Roller height in breaking tidal bores as function of the Froude number ($Fr = (V_1 + U)/(g \times d_1)^{1/2}$)—Comparison between breaking tidal bore data and Eq. (5) (black solid line) and Eq. (6) (red dashed line)



5 How can better flow analogies help?

This study clearly shows that more work needs to be done to elucidate the physics of the unsteady motion of a breaking roller. The metrology is clearly an issue to get accurate and reliable physical measurements in this rapidly-varied aerated turbulent flow. The scale effects are also a point to be addressed, with a close look at the differences due to the water salinity (tap water, saltwater, seawater). Some practice, such as the use of the Hinze’s [89] scale, are also believed to be misleading, as the theory was originally developed under assumptions not valid in the case of breaking waves. The analogy between hydraulic jumps, breaking tidal bores and breaking waves may be more appropriate in order to deduce quantities aimed at a modelling effort.

A stationary hydraulic jump is the sudden transition from a high-velocity free-surface flow impinging into a slower open channel flow. The rapid transition, called the roller, is characterised by spray and splashing with a highly fluctuating free-surface, together with highly-aerated turbulent flow structures within, and a large amount of energy dissipation takes place [5]. The application of the energy principle across the roller gives an expression of the energy dissipation. For a smooth horizontal rectangular channel and assuming hydrostatic pressure upstream and downstream of the roller, the rate of energy dissipation is [4, 21]:

$$\frac{\Delta E}{E_1} = \frac{(\sqrt{1 + 8 \times Fr^2} - 3)^3}{16 \times (\sqrt{1 + 8 \times Fr^2} - 1) \times (1 + \frac{1}{2} \times Fr^2)} \tag{7}$$

where E_1 is the upstream total energy: $E_1 = d_1 + (V_1)^2/(2 \times g)$. The rate of energy dissipation may exceed 70 % for $Fr > 9$ [32, 88]. However a non-breaking undular jump is observed at low Froude numbers. The transition from a stationary undular jump into a jump with a marked breaking roller takes place with the progressive apparition of characteristic three-dimensional flow features with increasing Froude numbers, including cross-waves

and cockscomb roller [46, 144]. A hydraulic jump with a fully-developed breaking roller is observed only for Froude numbers greater than 2–4 [35, 158]. Thus a stationary jump might not be truly representative of a spilling breaker, typically observed for $Fr < 2$.

It is believed that a more relevant analogy is the tidal breaking bore, as seen in Fig. 2b. A breaking bore with a quasi-two-dimensional roller is observed for Froude numbers greater than 1.4–1.6 [104, 115], although localised form of breaking might appear for Froude numbers above 1.3–1.4, including shock waves upstream of and limited breaking at the first wave crest [37, 173]. In the field, tidal bores are typically observed for Froude numbers less than 2.5, as shown in Table 3. As a further illustration, the Froude number was estimated to be about 2 for the bore seen in Fig. 2b2. Based upon basic energy considerations, the power dissipated in the bore roller may be estimated as (Appendix 2):

$$P_d = \rho \times g^{3/2} \times d_1^{5/2} \times L \times Fr \times \frac{(\sqrt{1 + 8 \times Fr^2} - 3)^3}{16 \times (\sqrt{1 + 8 \times Fr^2} - 1)} \tag{8}$$

where P_d is in Watts, L is the transverse length of the bore roller and where $E_1 = d_1 + (V_1 + U)^2 / (2 \times g)$ for a tidal bore. For the tidal bore seen in Fig. 2b2, the power dissipated was about: $P_d \approx 160$ MW. When a tidal bore propagates upstream in a sloping channel, experimental observations showed a complex transformation of a bore into a stationary hydraulic jump [30, 40]. In laboratory, the transformation could last from 5 to 10 min up to more than 20 min. At full scale, the duration of the process would be much longer, based upon a Froude similitude scaling, but the physical process remains poorly understood.

Even if the external forces generating the final roller are different in the flows considered in this study, the general aspect of the turbulent aerated bores seem visually similar in terms of lengths scales, intensities and aeration. Indeed, looking at the general hydrodynamic features of the flows presented in the literature, the roller region results in a sequence of splash-ups, inducing large-scale horizontal vortices. Considering the description of the splashing hydrodynamics in breaking waves (e.g. [18, 119, 132]), the roller region is roughly composed of 3–4 large horizontal vortices, which is consistent with experimental observations in tidal bores for $Fr < 2$. All the experimental studies, whatever the flow, indicated the capacity of successive

Table 3 Detailed field observations of tidal bores

Reference	River/Estuary	Date	Bore type	d_1 (m)	V_1 (m/s)	U (m/s)	Fr
Wolanski et al. [183]	Daly	2/07/2003	Undular	1.50	0.15	4.7	1.04
Simpson et al. [163]	Dee	6/09/2003	Breaking	0.72	0.15	4.1	1.79
Chanson et al. [50]	Garonne	10/09/2010	Undular	1.77	0.33	4.5	1.30
		11/09/2010	Undular	1.81	0.30	4.2	1.20
Mouaze et al. [138]	Sélune	24/09/2010	Breaking	0.38	0.86	2.0	2.35
		25/09/2010	Breaking	0.33	0.59	2.0	2.48
Reungoat et al. [154]	Garonne	7/06/2012 am	Undular	2.72	0.68	3.8	1.02
		7/06/2012 pm	Undular	2.65	0.59	4.6	1.19
Furgerot et al. [80]	Sée	7/05/2012	Undular	0.90	0.40	3.2	1.39
Reungoat et al. [155]	Garonne	13/10/2013	Undular	2.05	0.26	4.3	1.27
Leng and Chanson [115]	Qiantang	6/09/2013	Breaking	1	–	3.6	2.1
Chanson [43]	Qiantang	12/10/2014	Breaking	2 to 2.5	–	4.5	2.00

Italic data rough estimate; (–) data not available

splash-ups to entrain air large quantities of air. The co-existence between the large-scale clockwise vortices and some smaller counter-clockwise vortices, generated by backward splashing and impingement occurring in between co-rotative vortices pairs, is reported in all the observations. These large eddies are responsible for the turbulent fluctuations of the shape of the rollers. All the observations indicated that both air entrainment, turbulent shear and vorticity are generated along the surface of the rollers and in the toe region. The total air volume is less important than the number of bubbles and their actual size distributions in the roller region. The study of the highly fluctuating dynamics of the roller region should then bring fruitful insight in the dynamics of the flow. The temporal evolution of this region is highly required to get a better description of the variation of the roller height and energy dissipation, as a function of time.

The quantification of some parameters may be improved and some physical description can be highlighted, using the most appropriate analogy (roller/tidal bore) rather than the one typically used (roller/hydraulic jump). The roller length and height have been found to be fairly similar between hydraulic jumps and tidal bores (Fig. 6), even comparing laboratory and field studies, thus free of scale effects. Considering the tidal bore analogy and the corresponding observations presented in Fig. 5, the length of the roller should be considered within $1.5 < L_r/h_r < 5$. The transition between breaking and non-breaking waves would take place for $Fr > 1.3$, as observed in tidal bores. It was shown that the same limit value was inaccurately attributed to the transition between undular and breaking hydraulic jumps, but most recent studies proved it to be for $Fr > 2$ in stationary jumps. It is also interesting to notice that the celerity of the bore region considered in tidal bores is the celerity of the toe [114, 115], and not the celerity of the crest as used in modelling studies. The celerity of a tidal bore is found to be different from the celerity of a solitary wave. In a wave current problem, the Froude number represents the ratio between the velocity of a wave travelling and that of the current. The definition of the Froude number, as given for tidal bores in Table 2, should then be useful for breaking waves studies. It is similar to the estimation based on the RTFN concept [62, 145], and should be appropriate since it would be suitable for any type of analogy (deep and shallow water breaking waves). It is noted that the celerity of the crest, considered by Okamoto and Basco [145] should be replaced by the celerity of the toe, c_{trough} being V_1 with the current notation.

This study also presents some acknowledged limitations. The current work cannot provide any definition of a criterion for breaking onset. Experimental studies do not focus on the initiation and evolution of the breaking region in tidal bores or hydraulic jumps. Estimations of the wave velocity during breaking can lead to substantial discrepancies [146] and remains a challenge. A steepening wave can propagate for a long distance before clearly breaking and developing a roller; so the crest kinematics still need to be elucidated in complex situations (3D, current, turbulence, wind, etc.). The transient evolution of the roller is crucial for future studies [115]. Future interests should also encompass bubble size distribution and dynamics, two-phase gas–liquid turbulence and vorticity generation in the roller region. Interestingly, tidal bore is itself also a great example of highly non-linear phenomenon, as the free-surface evolution of the undulations observed in rivers and laboratories do not show any accordance with classical wave theories (cnoidal, solitary, Stokes). Analogies are complicated both ways.

6 Conclusions

In this study, we analysed and discussed the different analogies proposed in the literature to model the breaking process of the waves in the surf zone. Numerical models not only need experimental data for rigorous and extensive validations, but also for development. Even the most up-to-date and

accurate numerical models are still limited by empirical aspects. So a better knowledge of the temporal and spatial evolution of the aerated region under breaking waves is crucial.

The quantities which are needed for most numerical models are a characteristic Froude number to detect the breaking process occurrence, the geometrical and dynamical characteristics of the roller (height, length, mean front slope angle, celerity), the energy dissipation and the bubble size distribution. Two features are reported to be of great importance in all experimental studies: the bubble size distribution and the bubble cloud void fraction, the latter being highly dependent on the accurate quantification of the number of bubbles. But this aspect of the flow remains a technical challenge for both the numerical models and experimental technics. A number of issues remain and definitive conclusions cannot be drawn. The actual best practices have been discussed and better estimations have been proposed based on recent experimental data sets. We showed in particular that measurements, performed in tidal bores will lead to improve the description of the bubble plumes. The authors believe that the unsteady evolution of a decelerating tidal bore, showing transition between a tidal bore to a stationary hydraulic jump [40], could bring intriguing insights into the processes involved in the highly non-linear problem of breaking waves.

Acknowledgments The authors thank their students, former students and co-workers for their work and input. The financial support of the Australian Research Council (Grant DP120100481) is acknowledged.

Appendix 1

See Table 4.

Table 4 Breaking waves, bores, surges and jumps: flow analogies in the literature

Analogy spilling breaker and steady breakers	Banner and Phillips [6, 7], Duncan [73, 74], Banner and Peregrine [8] Cointe and Tulin [59] Lin and Rockwell [121] Dabiri and Gharib [63]
Analogy breaking wave and Plunging jet	Cipriano and Blanchard [56] Hubbard et al. [93] Chanson and Cummings [44] Oguz et al. [143] Chanson et al. [47, 48] Salter et al. [160]
Analogy spilling breaker and hydraulic jump	Longuet-Higgins [123] Peregrine and Svendsen [147] Madsen [128] Brocchini and Peregrine [23, 24]
Analogy spilling breaker and bore/positive surge	Longuet-Higgins [123] Peregrine and Svendsen [147] Brocchini and Peregrine [24]
Analogy breaking bore/positive surge and hydraulic jumps	ALL Hydraulics Textbooks, dealing with open channel flows, as well as: Darcy and Bazin [65] Stoker [164] Tricker [174] Henderson [88] Lighthill [118] Chanson [32, 41]
Other analogies—spilling breaker and density current	Longuet-Higgins and Turner [124]

Appendix 2: Basic momentum and energy considerations for bores and jumps

A bore is an abrupt rise in water depth (Fig. 1) and its front may be analysed as a hydraulic jump in translation [41, 118, 174]. In a system of reference in translation with the bore front, the integral form of the continuity and momentum equations gives a relationship between the cross-section area upstream and downstream of the roller, A_1 and A_2 respectively, and the upstream Froude number Fr_1 [114]

$$Fr_1^2 = \frac{1}{2} \times \frac{A_2}{A_1} \times \frac{B_1}{B} \times \left(\left(2 - \frac{B'}{B} \right) + \frac{B'}{B} \times \frac{A_2}{A_1} \right) + \frac{A_2}{A_2 - A_1} \times \frac{F_{\text{fric}} - W \times \sin \theta}{\rho \times g \times \frac{A_1^2}{B}} \quad (9)$$

where Fr_1 is the bore Froude number: $Fr = (U + V_1)/(g \times A_1/B_1)^{1/2}$, V is the cross-sectional averaged velocity positive downstream as shown in Fig. 1, U is the bore celerity positive upstream, the channel cross-sectional area A measured perpendicular to the flow direction, ρ is the water density, g is the gravity acceleration, F_{fric} is the friction force, W is the weight force, θ the angle between the bed slope and horizontal, and the subscripts 1 and 2 refer to the flow conditions immediately before and after the bore roller respectively (Fig. 1). In Eq. (9), B and B' are characteristic widths functions of the bathymetry:

$$B = \frac{A_2 - A_1}{d_2 - d_1} \quad (10)$$

$$B' = \frac{\int_{A_1}^{A_2} \int \rho \times g \times (d_2 - z) \times dA}{\frac{1}{2} \times \rho \times g \times (d_2 - d_1)^2} \quad (11)$$

with d the flow depth (Fig. 1b). For a smooth rectangular horizontal channel, Eq. (9) yields to the Bélanger equation:

$$\frac{d_2}{d_1} = \frac{1}{2} \times \left(\sqrt{1 + 8 \times Fr_1^2} - 1 \right) \text{ Smooth horizontal rectangular channel} \quad (12)$$

where d_1 and d_2 are respectively the upstream and downstream flow depth, and Fr_1 simplifies into: $Fr_1 = (U + V_1)/(g \times d_1)^{1/2}$ (Fig. 1). First presented in 1841 [12, 36], Eq. (12) is inappropriate in an irregular channel [41]. The roller height h_r is in first approximation: $h_r = d_2 - d_1$ and Eq. (12) may be rewritten as:

$$Fr_1^2 = \frac{1}{2} \times \left(\frac{d_2 - d_1}{d_1} \right)^2 + \frac{3}{2} \frac{d_2 - d_1}{d_1} \text{ Smooth horizontal rectangular channel} \quad (13)$$

Note that the above development (Eq. 9, 12 and 13) assumes implicitly that the bore celerity is uniform and the roller shape two-dimensional. Field and laboratory observations suggested that these assumptions are simplistic [114].

The application of the energy principle across the bore roller gives an expression of the energy dissipation [4, 21]:

$$\Delta E = d_1 + \frac{(V_1 + U)^2}{2 \times g} - \left(d_2 + \frac{(V_2 + U)^2}{2 \times g} \right) \tag{14}$$

assuming hydrostatic pressure upstream and downstream. For a smooth horizontal rectangular channel, the rate of energy dissipation becomes [5]:

$$\frac{\Delta E}{E_1} = \frac{\left(\sqrt{1 + 8 \times Fr_1^2} - 3 \right)^3}{16 \times \left(\sqrt{1 + 8 \times Fr_1^2} - 1 \right) \times \left(1 + \frac{1}{2} \times Fr_1^2 \right)} \tag{15}$$

where $E_1 = d_1 + (V_1 + U)^2 / (2 \times g)$. The rate of energy dissipation ranges from 0 for $Fr_1 = 1$ to more than 70 % for $Fr_1 > 9$ [32, 88]. The power dissipated in the bore is:

$$P_d = \rho \times g \times (V_1 + U) \times d_1 \times L \times \Delta E \tag{16}$$

where L is the transverse length of the bore roller. In the above equations, the solution for a stationary hydraulic jump is obtained for $U = 0$.

References

1. Angelova MD, Huq P (2012) Characteristics of bubble clouds at various wind speeds. *J Geophys Res* 117:C03036. doi:10.1029/2011JC007442
2. Babb AF, Aus HC (1981) Measurements of air in flowing water. *J Hydraul Div ASCE* 107(12):1615–1630
3. Bacigaluppi P, Ricchiuto M, Bonneton P (2014) Upwind stabilized finite element modelling of non-hydrostatic wave breaking and run-up. Research Report INRIA, RR-8536, <https://hal.inria.fr/hal-00990002v3>
4. Bakhmeteff BA (1912) *O Neravnomernom Dvijenii Jidkosti v Otkrytom Rusle*. (Varied Flow in Open Channel.) St Petersburg, Russia (in Russian)
5. Bakhmeteff BA (1932) *Hydraulics of open channels*, 1st edn. McGraw-Hill, New York
6. Banner ML, Phillips OM (1974) On the incipient breaking of small scale waves. *J Fluid Mech* 65:647–656
7. Banner ML, Melville WK (1976) On the separation of air flow over water waves. *J Fluid Mech* 77:825–891
8. Banner ML, Peregrine DH (1993) Wave breaking in deep water. *Annu Rev Fluid Mech* 25:373–397
9. Basco DR (1985) A qualitative description of wave breaking. *J Waterw Port Coast Ocean Eng* 111(2):171–188
10. Battjes JA (1988) Surf-zone dynamics. *Ann Rev Fluid Mech* 20:257–293
11. Bazin H (1865) *Recherches Expérimentales sur la Propagation des Ondes*. (‘Experimental Research on Wave Propagation.’) Mémoires présentés par divers savants à l’Académie des Sciences, Paris, France, Vol. 19, pp. 495–644 (in French)
12. Bélanger JB (1841) “Notes sur l’Hydraulique.” (‘Notes on Hydraulic Engineering.’) *Ecole Royale des Ponts et Chaussées*, Paris, France, session 1841–1842, 223 pp (in French)
13. Bjørkavåg M, Kalisch H (2011) Wave breaking in Boussinesq models for undular bores. *Phys Lett A* 375:1570–1578
14. Blenkinsopp CE, Chaplin JR (2007) Void fraction measurements in breaking waves. *Proc R Soc A* 463:3151–3170. doi:10.1098/rspa.2007.1901
15. Blenkinsopp CE, Chaplin JR (2010) Bubble size measurements in breaking waves using optical fiber phase detection probes. *J Ocean Eng* 35(2):388–401
16. Blenkinsopp CE, Chaplin JR (2011) Void fraction measurements and scale effects in breaking waves in freshwater and seawater. *Coast Eng* 58:417–428
17. Bombardelli FA (2012) Computational multi-phase fluid dynamics to address flows past hydraulic structures. Proceedings of 4th IAHR International Symposium on Hydraulic Structures, APRH—

- Associação Portuguesa dos Recursos Hídricos (Portuguese Water Resources Association), J. Matos, S. Pagliara & I. Meireles Eds., 9–11 February 2012, Porto, Portugal, Paper 2, 19 pages (CD-ROM)
18. Bonmarin P (1989) Geometric properties of deep-water breaking waves. *J Fluid Mech* 209:405–433
 19. Boussinesq JV (1877) Essai sur la Théorie des Eaux Courantes. ('Essay on the Theory of Water Flow.') Mémoires présentés par divers savants à l'Académie des Sciences, Paris, France, Vol. 23, Série 3, No. 1, supplément 24, pp. 1–680 (**in French**)
 20. Bowyer PA (2001) Video measurements of near-surface bubble spectra. *J Geophys Res* 106(C7):14179–14190
 21. Bresse JA (1868) Cours de Mécanique Appliquée Professe à l'École Impériale des Ponts et Chaussées. (Course in Applied Mechanics lectured at the Pont-et-Chaussées Engineering School.) Gauthier-Villars, Paris, France, 586 p (**in French**)
 22. Brocchini M (2013) A reasoned overview on Boussinesq-type models: the interplay between physics, mathematics and numerics. *Proc R Soc A* 469:20130496
 23. Brocchini M, Peregrine DH (2001) The dynamics of strong turbulence at free surfaces. Part 1. Description. *J Fluid Mech* 449:225–254
 24. Brocchini M, Peregrine DH (2001) The dynamics of strong turbulence at free surfaces. Part 2. Free-surface boundary conditions. *J Fluid Mech* 449:255–290
 25. Callaghan AH, Stokes MD, Deane GB (2014) The effect of water temperature on air entrainment, bubble plumes, and surface foam in a laboratory breaking-wave analog. *J Geophys Res Ocean*. doi:[10.1002/2014JC010351](https://doi.org/10.1002/2014JC010351)
 26. Carrica PM, Drew D, Bonetto F, Lahey RT Jr (1999) A polydisperse model for bubbly two-phase flow around a surface ship. *Int J Multiph Flow* 25:257–305
 27. Cartellier A, Achard JL (1991) Local phase detection probes in fluid/fluid two-phase flows. *Rev Sci Instrum* 62(2):279–303
 28. Cartmill J, Su M (1993) Bubble size distribution under saltwater and freshwater breaking waves. *Dyn Atmos Oceans* 20:25–31. doi:[10.1016/0377-0265\(93\)90046-A](https://doi.org/10.1016/0377-0265(93)90046-A)
 29. Chachereau Y, Chanson H (2011) Bubbly flow measurements in hydraulic jumps with small inflow Froude numbers. *Int J Multiph Flow* 37(6):555–564. doi:[10.1016/j.ijmultiphaseflow.2011.03.012](https://doi.org/10.1016/j.ijmultiphaseflow.2011.03.012)
 30. Chanson H (1996) Free-surface flows with near-critical flow conditions. *Can J Civ Eng* 23(6):1272–1284
 31. Chanson H (1997) Air bubble entrainment in free-surface turbulent shear flows. Academic Press, London
 32. Chanson H (2004) The hydraulics of open channel flow: an introduction, 2nd edn. Butterworth-Heinemann, Oxford
 33. Chanson H (2005) Air–water and momentum exchanges in unsteady surging waters: an experimental study. *Exp Thermal Fluid Sci* 30(1):37–47
 34. Chanson H (2007) Bubbly flow structure in hydraulic jump. *Eur J Mech B/Fluids* 26(3):367–384. doi:[10.1016/j.euromechflu.2006.08.001](https://doi.org/10.1016/j.euromechflu.2006.08.001)
 35. Chanson H (2009) Turbulent air–water flows in hydraulic structures: dynamic similarity and scale effects. *Environ Fluid Mech* 9(2):125–142. doi:[10.1007/s10652-008-9078-3](https://doi.org/10.1007/s10652-008-9078-3)
 36. Chanson H (2009) Development of the Bélanger equation and backwater equation by Jean-Baptiste Bélanger (1828). *J Hydraul Eng ASCE* 135(3):159–163. doi:[10.1061/\(ASCE\)0733-9429\(2009\)135:3\(159\)](https://doi.org/10.1061/(ASCE)0733-9429(2009)135:3(159))
 37. Chanson H (2010) Undular tidal bores: basic theory and free-surface characteristics. *J Hydraul Eng ASCE* 136(11):940–944. doi:[10.1061/\(ASCE\)HY.1943-7900.0000264](https://doi.org/10.1061/(ASCE)HY.1943-7900.0000264)
 38. Chanson H (2010) Unsteady turbulence in tidal bores: effects of bed roughness. *J Waterw Port Coast Ocean Eng ASCE* 136(5):247–256. doi:[10.1061/\(ASCE\)WW.1943-5460.0000048](https://doi.org/10.1061/(ASCE)WW.1943-5460.0000048)
 39. Chanson H (2010) Convective transport of air bubbles in strong hydraulic jumps. *Int J Multiph Flow* 36(10):798–814. doi:[10.1016/j.ijmultiphaseflow.2010.05.006](https://doi.org/10.1016/j.ijmultiphaseflow.2010.05.006)
 40. Chanson H (2011) Turbulent shear stresses in hydraulic jumps and decelerating surges: an experimental study. *Earth Surf Process Landf* 36(2):180–189. doi:[10.1002/esp.2031](https://doi.org/10.1002/esp.2031)
 41. Chanson H (2012) Momentum considerations in hydraulic jumps and bores. *J Irrig Drain Eng ASCE* 138(4):382–385. doi:[10.1061/\(ASCE\)IR.1943-4774.0000409](https://doi.org/10.1061/(ASCE)IR.1943-4774.0000409)
 42. Chanson H (2013) Hydraulics of aerated flows: Qui Pro Quo?. *J Hydraul Res, IAHR*. Invited Vision paper, 51(3): 223–243. doi: [10.1080/00221686.2013.795917](https://doi.org/10.1080/00221686.2013.795917)
 43. Chanson H (2016) Atmospheric noise of a breaking tidal bore. *J Acoust Soc Am* 139(1):12–20. doi:[10.1121/1.4939113](https://doi.org/10.1121/1.4939113)
 44. Chanson H, Cummings PD (1994) Effects of plunging breakers on the gas contents in the oceans. *Mar Technol Soc J* 28(3):22–32

45. Chanson H, Gualtieri C (2008) Similitude and scale effects of air entrainment in hydraulic jumps. *J Hydraul Res* 46(1):35–44
46. Chanson H, Montes JS (1995) Characteristics of undular hydraulic jumps. Experimental apparatus and flow patterns. *J Hydraul Eng ASCE* 121(2):129–144
47. Chanson H, Aoki S, Maruyama M (2002) Unsteady air bubble entrainment and detrainment at a plunging breaker: dominant time scales and similarity of water level variations. *Coast Eng* 46(2):139–157
48. Chanson H, Aoki S, Hoque A (2006) Bubble entrainment and dispersion in plunging jet flows: freshwater versus seawater. *J Coast Res* 22(3):664–677. doi:[10.2112/03-0112.1](https://doi.org/10.2112/03-0112.1)
49. Chanson H, Brattberg T (2000) Experimental study of the air–water shear flow in a hydraulic jump. *Int J Multiph Flow* 26(4):583–607
50. Chanson H, Reungoat D, Simon B, Lubin P (2011) High-frequency turbulence and suspended sediment concentration measurements in the Garonne River Tidal Bore. *Estuar Coast Shelf Sci* 95(2–3):298–306. doi:[10.1016/j.ecss.2011.09.012](https://doi.org/10.1016/j.ecss.2011.09.012)
51. Chanson H, Toi YH (2015) Physical modelling of breaking tidal bores: comparison with prototype data. *J Hydraul Res IAHR* 53(2):264–273. doi:[10.1080/00221686.2014.989458](https://doi.org/10.1080/00221686.2014.989458)
52. Chen G, Kharif C, Zaleski S, Li J (1999) Two-dimensional Navier–Stokes simulation of breaking waves. *Phys Fluids* 11(1):121–133
53. Cheng J, Wang P (2015) Extracting turbulence under breaking waves in the surf zone. *J Waterw Port Coast Ocean Eng.* doi:[10.1061/\(ASCE\)WW.1943-5460.0000307](https://doi.org/10.1061/(ASCE)WW.1943-5460.0000307)
54. Christensen ED, Walstra D-J, Emerat N (2002) Vertical variation of the flow across the surf zone. *Coast Eng* 45:169–198
55. Cienfuegos R, Barthélemy E, Bonneton P (2010) Wave-breaking model for boussinesq-type equations including roller effects in the mass conservation equation. *J Waterw Port Coast Ocean Eng* 136(1):10–26
56. Cipriano RJ, Blanchard DC (1981) Bubble and aerosol spectra produced by a laboratory ‘breaking wave’. *J Geophys Res* 86(C9):8085–8092
57. Clift R, Grace JR, Weber ME (1978) Bubbles, drops, and particles. Academic Press, San Diego
58. Coakley DB, Haldeman PM, Morgan DG, Nicolas KR, Penndorf DR, Wetzel LB, Weller CS (2001) Electromagnetic scattering from large steady breaking waves. *Exp Fluids* 30(5):479–487. doi:[10.1007/s003480000220](https://doi.org/10.1007/s003480000220)
59. Coince R, Tulin MP (1994) A theory of steady breakers. *J Fluid Mech* 216:1–20
60. Cox DT, Shin S (2003) Laboratory measurements of void fraction and turbulence in the Bore Region of surf zone waves. *J Eng Mech ASCE* 129(10):1197–1205
61. Crowe CT, Schwarzkopf JD, Sommerfeld M, Tsuji Y (2011) Multiphase flows with droplets and particles, 2nd edn. Boca Raton, CRC Press
62. D’Alessandro F, Tomasicchio GR (2008) The BCI criterion for the initiation of breaking process in Boussinesq-type equations wave models. *Coast Eng* 55:1174–1184
63. Dabiri D, Gharib M (1997) Experimental investigation of the vorticity generation within a spilling water wave. *J Fluid Mech* 330:113–139
64. Dahl PH, Jessup AT (1995) On bubble clouds produced by breaking waves: an event analysis of ocean acoustic measurements. *J Geophys Res* 100(C3):5007–5020. doi:[10.1029/94JC03019](https://doi.org/10.1029/94JC03019)
65. Darcy HPG, Bazin H (1865) *Recherches Hydrauliques.* (Hydraulic Research.) Imprimerie Impériales, Paris, France, Parties 1ère et 2ème (in French)
66. Deane G (1997) Sound generation and air entrainment by breaking waves in the surf zone. *J Acoust Soc Am* 102(5):2671–2689. doi:[10.1121/1.420321](https://doi.org/10.1121/1.420321)
67. Deane G, Stokes MD (2002) Scale dependence of bubble creation mechanisms in breaking waves. *Nature* 418:839–844
68. Derakhti M, Kirby JT (2014) Bubble entrainment and liquid–bubble interaction under unsteady breaking waves. *J Fluid Mech* 761:464–506. doi:[10.1017/jfm.2014.637](https://doi.org/10.1017/jfm.2014.637)
69. Docherty NJ, Chanson H (2012) Physical modelling of unsteady turbulence in breaking tidal bores. *J Hydraul Eng ASCE* 138(5):412–419. doi:[10.1061/\(ASCE\)HY.1943-7900.0000542](https://doi.org/10.1061/(ASCE)HY.1943-7900.0000542)
70. Drazen DA, Melville WK, Lenain L (2008) Inertial scaling of dissipation in unsteady breaking waves. *J Fluid Mech* 611:307–332
71. Drew DA (1983) Mathematical modeling of two-phase flow. *Annu Rev Fluid Mech* 1983(15):261–291
72. Drew DA, Passman SL (1999). *Theory of Multicomponent Fluids.* Applied Mathematical Sciences, Vol. 135, Springer: New York, doi:[10.1007/b97678](https://doi.org/10.1007/b97678)
73. Duncan JH (1981) An experimental investigation of breaking waves produced by a towed hydrofoil. *Proc R Soc Lond A* 377:331–348
74. Duncan JH (2001) Spilling breakers. *Annu Rev Fluid Mech* 33:519–547

75. Esmaeeli A, Tryggvason G (1996) An inverse energy cascade in two-dimensional low Reynolds number bubbly flows. *J Fluid Mech* 314:315–330
76. Falvey HT (1990) Cavitation in chutes and spillways. US Bureau of Reclamation Engineering Monograph, No. 42, Denver, Colorado, USA
77. Farahani RJ, Dalrymple RA (2014) Three-dimensional reversed horseshoe vortex structures under broken solitary waves. *Coast Eng* 91:261–279
78. Favre H (1935) Etude Théorique et Expérimentale des Ondes de Translation dans les Canaux Découverts. ('Theoretical and Experimental Study of Travelling Surges in Open Channels.') Dunod, Paris, France (in French)
79. Führboter A (1970). Air entrainment and energy dissipation in breakers. 12th International Conference on Coastal Engineering. <https://journals.tdl.org/icce/index.php/icce/article/view/2628>
80. Furgerot L, Mouaze D, Tessier B, Perez L, Haquin S (2013) Suspended Sediment Concentration in Relation to the Passage of a Tidal Bore (Sée River Estuary, Mont Saint Michel, NW France). *Proc. Coastal Dynamics 2013*, Arcachon, France, 24–28 June, pp. 671–682
81. Galinat S, Risso F, Masbernat O, Guiraud P (2007) Dynamics of drop breakup in inhomogeneous turbulence at various volume fractions. *J Fluid Mech* 578:85–94. doi:10.1017/S0022112007005186
82. Gemmrich J (2010) Strong turbulence in the wave crest region. *J Phys Oceanogr* 40:583–595. doi:10.1175/2009JPO4179.1
83. Gemmrich JR, Farmer DM (2004) Near-surface turbulence in the presence of breaking waves. *J Phys Oceanogr* 34:1067–1086
84. Gomez-Gesteira M, Rogers BD, Dalrymple RA, Crespo AJC (2010) State-of-the-art of classical SPH for free-surface flows. *J Hydraul Res* 48(S1):6–27. doi:10.1080/00221686.2010.9641242
85. Govender K, Mocke GP, Alport MJ (2002) Video-imaged surf zone wave and roller structures and flow fields. *J Geophys Res* 107(C7):3072. doi:10.1029/2000JC000755
86. Gualtieri C, Chanson H (2010) Effect of Froude number on bubble clustering in a hydraulic jump. *J Hydraul Res IAHR* 48(4):504–508
87. Haller MC, Catalán PA (2010) Remote sensing of wave roller lengths in the laboratory. *J Geophys Res* 114:C07022. doi:10.1029/2008JC005185
88. Henderson FM (1966) Open channel flow. MacMillan Company, New York
89. Hinze JO (1955) Fundamentals of the hydrodynamic mechanism of slitting in dispersion processes. *J Am Inst Chem Eng* 1:289–295
90. Hoque A, Aoki S-I (2005) Distributions of void fraction under breaking waves in the surf zone. *Ocean Eng* 32:1829–1840
91. Hornung HG, Willert C, Turner S (1995) The flow field downstream of a hydraulic jump. *J Fluid Mech* 287:299–316
92. Hoyt JW, Sellin RHJ (1989) Hydraulic jump as 'mixing layer'. *J Hydraul Eng ASCE* 115(12):1607–1614
93. Hubbard DW, Griffin OM, Peltzer RD (1987) Foam generation and air entrainment near a free surface. Naval Research Laboratory Memorandum Report 6038, Washington D.C., USA
94. Hwung HH, Chyan JM, Chung YC (1992) Energy dissipation and air bubbles mixing inside surf zone. Proceedings of 23rd International Conference on Coastal Engineering, ASCE, Venice, Italy, Vol. 1, Chap. 22, pp. 308–321
95. Iafrafi A (2009) Numerical study of the effects of the breaking intensity on wave breaking flows. *J Fluid Mech* 622:371–411
96. Iafrafi A (2011) Energy dissipation mechanisms in wave breaking processes: spilling and highly aerated plunging breaking events. *J Geophys Res* 116:C07024. doi:10.1029/2011JC007038
97. Jansen PCM (1986) Laboratory observations of the kinematics in the aerated region of breaking waves. *Coast Eng* 9:453–477
98. Kalvoda PM, Xu L, Wu J (2003) Macrobubble clouds produced by breaking wind waves: a laboratory study. *J Geophys Res* 108(C6):3207. doi:10.1029/1999JC000265
99. Katz Y, Horev E, Wygnanski I (1992) The forced turbulent wall jet. *J Fluid Mech* 242:577–609
100. Kazolea M, Delis AI, Synolakis CE (2014) Numerical treatment of wave breaking on unstructured finite volume approximations for extended Boussinesq-type equations. *J Comput Phys* 271:281–305
101. Kimmoun O, Branger H (2007) A particle image velocimetry investigation on laboratory surf-zone breaking waves over a sloping beach. *J Fluid Mech* 588:353–397
102. Kiger KT, Duncan JH (2012) Air-entrainment mechanisms in plunging jets and breaking waves. *Ann Rev Fluid Mech* 44:563–596
103. Kennedy AB, Chen Q, Kirby JT, Dalrymple RA (2000) Boussinesq modeling of wave transformation, breaking and run-up. I: one dimension. *ASCE. J Waterw Port Coast Ocean Eng* 126(1):48–56

104. Koch C, Chanson H (2008) Turbulent mixing beneath an undular bore front. *J Coast Res* 24(4):999–1007. doi:[10.2112/06-0688.1](https://doi.org/10.2112/06-0688.1)
105. Koch C, Chanson H (2009) Turbulence measurements in positive surges and bores. *J Hydraul Res IAHR* 47(1):29–40. doi:[10.3826/jhr.2009.2954](https://doi.org/10.3826/jhr.2009.2954)
106. Kucukali S, Chanson H (2008) Turbulence measurements in hydraulic jumps with partially-developed inflow conditions. *Exp Thermal Fluid Sci* 33(1):41–53. doi:[10.1016/j.expthermflusci.2008.06.012](https://doi.org/10.1016/j.expthermflusci.2008.06.012)
107. Labourasse E, Lacanette D, Toutant A, Lubin P, Vincent S, Lebaigue O, Caltagirone J-P, Sagaut P (2007) Towards large eddy simulation of isothermal two-phase flows: governing equations and a priori tests. *Int J Multiph Flow* 33(1):1–39
108. Lakehal D, Liovic P (2011) Turbulence structure and interaction with steep breaking waves. *J Fluid Mech* 674:522–577. doi:[10.1017/jfm.2011.3](https://doi.org/10.1017/jfm.2011.3)
109. Lamarre E, Melville WK (1991) Air entrainment and dissipation in breaking waves. *Nature* 351:469–472. doi:[10.1038/351469a0](https://doi.org/10.1038/351469a0)
110. Lamarre E, Melville WK (1992) Instrumentation for the measurement of void-fraction in breaking waves: laboratory and field results. *IEEE J Ocean Eng* 17(2):204–215. doi:[10.1109/48.126977](https://doi.org/10.1109/48.126977)
111. Lamarre E, Melville WK (1994) Void-fraction measurements and sound-speed fields in bubble plumes generated by breaking waves. *J Acoust Soc Am* 95(3):1317–1328. doi:[10.1121/1.408572](https://doi.org/10.1121/1.408572)
112. Leandro J, Carvalho R, Chachereau Y, Chanson H (2012) Estimating void fraction in a hydraulic jump by measurements of pixel intensity. *Exp Fluids* 52(5):1307–1318. doi:[10.1007/s00348-011-1257-1](https://doi.org/10.1007/s00348-011-1257-1)
113. Leifer I, Caulliez G, de Leeuw G (2006) Bubbles generated from wind-steepened breaking waves: 2. Bubble plumes, bubbles, and wave characteristics. *J Geophys Res* 111:C06021. doi:[10.1029/2004JC002676](https://doi.org/10.1029/2004JC002676)
114. Leng X, Chanson H (2015) Turbulent advances of a breaking bore: preliminary physical experiments. *Exp Thermal Fluid Sci* 62:70–77. doi:[10.1016/j.expthermflusci.2014.12.002](https://doi.org/10.1016/j.expthermflusci.2014.12.002)
115. Leng X, Chanson H (2015) Breaking bore: physical observations of roller characteristics. *Mech Res Commun* 65:24–29. doi:[10.1016/j.mechrescom.2015.02.008](https://doi.org/10.1016/j.mechrescom.2015.02.008)
116. Leng X, Chanson H (2016) Coupling between free-surface fluctuations, velocity fluctuations and turbulent reynolds stresses during the upstream propagation of positive surges, bores and compression waves. *Environ Fluid Mech* 16(4):695–719. doi:[10.1007/s10652-015-9438-8](https://doi.org/10.1007/s10652-015-9438-8)
117. Lennon JM, Hill DF (2006) Particle image velocimetry measurements of undular and hydraulic jumps. *J Hydraul Eng* 132(12):1283–1294
118. Lighthill J (1978) *Waves in fluids*. Cambridge University Press, Cambridge
119. Lim H-J, Chang K-A, Huang Z-C, Na B (2015) Experimental study on plunging breaking waves in deep water. *J Geophys Res Oceans* 120:2007–2049. doi:[10.1002/2014JC010269](https://doi.org/10.1002/2014JC010269)
120. Lin C, Hwung HH (1992) External and internal flow fields of plunging breakers. *Exp Fluids* 12:229–237
121. Lin JC, Rockwell D (1995) Evolution of a quasi-steady breaking wave. *J Fluid Mech* 302:29–44
122. Loewen MR, O’Dor MA, Skafel MG (1996) Bubbles entrained by mechanically generated breaking waves. *J Geophys Res: Oceans* 101(C9):20759–20769
123. Longuet-Higgins MS (1973) A model of flow separation at a free surface. *J. Fluid Mech* 57(1):129–148
124. Longuet-Higgins MS, Turner JS (1974) An ‘entraining plume’ model of a spilling breaker. *J. Fluid Mech* 63(1):1–20
125. Lubin P, Vincent S, Abadie S, Caltagirone J-P (2006) Three-dimensional large eddy simulation of air entrainment under plunging breaking waves. *Coast Eng* 53(8):631–655
126. Lubin P, Glockner S (2015) Numerical simulations of three-dimensional plunging breaking waves: generation and evolution of aerated vortex filaments. *J Fluid Mech* 767:364–393. doi:[10.1017/jfm.2015.62](https://doi.org/10.1017/jfm.2015.62)
127. Ma G, Shi F, Kirby JT (2011) A polydisperse two-fluid model for surf zone bubble simulation. *J Geophys Res* 116:C05010
128. Madsen PA (1981) A model for a turbulent bore. Ph.D. Thesis, Tech. Univ. of Denmark, Inst. of Hydrodynamics and Hyd. Eng., Copenhagen, Denmark, 149 pages. (also Series Paper No. 28, Tech. Univ. of Denmark, Inst. of Hydrodynamics and Hyd. Eng., Copenhagen, Denmark, 149 pages.)
129. Melville WK (1996) The role of surface-wave breaking in air–sea interaction. *Annu Rev Fluid Mech* 28:279–321
130. Melville WK, Veron F, White CJ (2002) The velocity field under breaking waves: coherent structures and turbulence. *J Fluid Mech* 454:203–233
131. Miller RL (1972) Study of air entrainment in breaking waves. *Am Geophys Union Trans EOS* 53:426
132. Miller RL (1976) Role of vortices in surf zone prediction: sedimentation and wave forces. In *Beach and Nearshore Sedimentation*, Edited by Richard A. Davis, Jr. and R. L. Ethington, 24: 92–114

133. Monahan EC (1993) Occurrence and evolution of acoustically relevant sub-surface bubble plumes and their associated, remotely monitorable, surface whitecaps". In: Kerman BR (ed) Natural physical sources of underwater sound. Kluwer, Dordrecht, pp 503–517
134. Moraga FJ, Carrica PM, Drew DA, Lahey RT Jr (2008) A sub-grid air entrainment model for breaking bow waves and naval surface ships. *Comput Fluids* 37:281–298
135. Mori N, Suzuki T, Kakuno S (2007) Experimental study of air bubbles and turbulence characteristics in the surf zone. *J Geophys Res* 112:C05014. doi:[10.1029/2006JC003647](https://doi.org/10.1029/2006JC003647)
136. Mori N, Kakuno S (2008) Aeration and bubble measurements of coastal breaking waves. *Fluid Dyn Res* 40:616–626
137. Mossa M, Tolve U (1998) Flow visualization in bubbly two-phase hydraulic jump. *J Fluids Eng, ASME* 120:160–165
138. Mouaze D, Chanson H, Simon B (2010) Field measurements in the tidal bore of the Sélune River in the Bay of Mont Saint Michel (September 2010). Hydraulic Model Report No. CH81/10, School of Civil Engineering, The University of Queensland, Brisbane, Australia
139. Murzyn F, Chanson H (2009) Free-surface fluctuations in hydraulic jumps: experimental observations. *Exp Thermal Fluid Sci* 33(7):1055–1064. doi:[10.1016/j.expthermflusci.2009.06.003](https://doi.org/10.1016/j.expthermflusci.2009.06.003)
140. Murzyn F, Mouaze D, Chaplin JR (2005) Optical fibre probe measurements of bubbly flow in hydraulic jumps. *Intl J Multiph Flow* 31(1):141–154
141. Musumeci RE, Svendsen IA, Veeramony J (2005) The flow in the surf zone: a fully nonlinear Boussinesq-type of approach. *Coast Eng* 52:565–598. doi:[10.1016/j.coastaleng.2005.02.007](https://doi.org/10.1016/j.coastaleng.2005.02.007)
142. Nadaoka K, Hino M, Koyano Y (1989) Structure of the turbulent flow field under breaking waves in the surf zone. *J Fluid Mech* 204:359–387
143. Oguz HN, Prosperetti A, Kolaini AR (1995) Air entrapment by a falling mass of water. *J Fluid Mech* 294:181–207
144. Ohtsu, I., Yasuda, Y., and Gotoh, H. (2001). Hydraulic condition for undular-jump formations. *J Hydraul Res IAHR*, 39(2), 203–209. Discussion: 2002 40 (3), 379–384
145. Okamoto T, Basco DR (2006) The relative trough Froude number for initiation of wave breaking: theory experiments and numerical model confirmation. *Coast Eng* 53:675–690
146. Peregrine DH (1983) Breaking waves on beaches. *Annu Rev Fluid Mech* 15:149–178
147. Peregrine DH, Svendsen IA (1978) Spilling breakers, bores and hydraulic jumps. *Proc Int Conf Coast Eng* 30:540–550
148. Prosperetti A (1988) Bubble-related ambient noise in the ocean. *J Acoust Soc Am* 84(3):1042–1054
149. Rajaratnam N (1962) An experimental study of air entrainment characteristics of the hydraulic jump. *J Inst Eng India* 42(7):247–273
150. Rajaratnam, N. (1965). The Hydraulic Jump as a Wall Jet. *Jl of Hyd. Div., ASCE*, Vol. 91, No. HY5, pp. 107–132. Discussion: Vol. 92, No. HY3, pp. 110–123 & Vol. 93, No. HY1, pp. 74–76
151. Rao NSL, Kobus HE (1971) Characteristics of self-aerated free-surface flows. *Water and waste water/ current research and practice*, vol 10. Eric Schmidt Verlag, Berlin
152. Rapp RJ, Melville WK (1990) Laboratory measurements of deep-water breaking waves. *Philos Trans R Soc Lond Ser A* 331:735–800. doi:[10.1098/rsta.1990.0098](https://doi.org/10.1098/rsta.1990.0098)
153. Resch FJ, Leutheusser HJ (1972) Le Ressaut Hydraulique: mesure de Turbulence dans la Région Diphasique. *Jl La Houille Blanche* 1(4):279–293 (**in French**)
154. Reungoat D, Chanson H, Caplain B (2014) Sediment processes and flow reversal in the undular tidal bore of the Garonne River (France). *Environ Fluid Mech* 14(3):591–616. doi:[10.1007/s10652-013-9319-y](https://doi.org/10.1007/s10652-013-9319-y)
155. Reungoat D, Chanson H, Keevil CE (2015) Field Measurements of Unsteady Turbulence in a Tidal Bore: the Garonne River in October 2013. *J Hydraul Res IAHR*. doi:[10.1080/00221686.2015.1021717](https://doi.org/10.1080/00221686.2015.1021717)
156. Rojas G, Loewen MR (2010) Void fraction measurements beneath plunging and spilling breaking waves. *J Geophys Res* 115:C08001. doi:[10.1029/2009JC005614](https://doi.org/10.1029/2009JC005614)
157. Rouse H, Siao TT, Nagaratnam S (1959) Turbulence characteristics of the hydraulic jump. *Trans ASCE* 124:926–950
158. Ryabenko, A.A. (1990). Conditions favorable to the existence of an undulating jump. *Gidrotekhnicheskoe Stroitel'stvo*, No. 12, pp. 29–34 (**in Russian**). (Translated in *Hydrotechnical Construction*, 1990, Plenum Publ., pp. 762–770)
159. Russell SO, Sheehan GJ (1974) Effect of entrained air on cavitation damage. *Can J Civil Eng* 1:97–107
160. Salter ME, Nilsson ED, Butcher A, Bilde M (2014) On the seawater temperature dependence of the sea spray aerosol generated by a continuous plunging jet. *J Geophys Res Atmos*. doi:[10.1002/2013JD021376](https://doi.org/10.1002/2013JD021376)

161. Schäffer HA, Madsen PA, Deigaard R (1993) A Boussinesq model for waves breaking in shallow water. *Coast Eng* 20:185–202
162. Shi F, Kirby JT, Ma G (2010) Modeling quiescent phase transport of air bubbles induced by breaking waves. *Ocean Model* 35:105–117
163. Simpson JH, Fisher NR, Wiles P (2004) Reynolds Stress and TKE Production in an Estuary with a tidal bore. *Estuar Coast Shelf Sci* 60(4):619–627
164. Stoker JJ (1957) *Water waves. The mathematical theory with applications*. New York, Interscience Publishers
165. Stokes MD, Deane GB (1999) A new optical instrument for the study of bubbles at high void fractions within breaking waves. *IEEE J Ocean Eng* 24(3):300–311
166. Stokes D, Deane G, Vagle S, Farmer D (2002) Measurements of large bubbles in open-ocean whitecaps. *Gas Transf Water Surf*, pp. 279–284. doi:[10.1029/GM127p0279](https://doi.org/10.1029/GM127p0279)
167. Svendsen IA (1984) Wave heights and set-up in a surf zone. *Coast Eng* 8:303–329
168. Svendsen IA (1984) Mass flux and undertow in a surf zone. *Coast Eng* 8:347–365
169. Taylor G (1934) The formation of emulsions in definable field of flow. *Proc R Soc A* 146:501–523
170. Thorpe SA (1982) On the clouds of bubbles formed by breaking wind-waves in deep water, and their role in air–sea gas transfer. *Philos Trans R Soc Lond A* 304:155–210. doi:[10.1098/rsta.1982.0011](https://doi.org/10.1098/rsta.1982.0011)
171. Tissier M, Bonneton P, Marche F, Lannes D (2012) A new approach to handle wave breaking in fully non-linear Boussinesq models. *Coast Eng* 67:54–66
172. Tonelli M, Petti M (2009) Hybrid finite volume-finite difference scheme for 2DH improved Boussinesq equations. *Coast Eng* 56:609–620
173. Treske A. (1994). Undular bores (favre-waves) in open channels—experimental studies. *J Hydraul Res. IAHR*, Vol. 32, No. 3, pp. 355–370. Discussion: Vol. 33, No. 3, pp. 274–278
174. Tricker RAR (1965) *Bores, breakers waves and wakes*. American Elsevier Publ. Co., New York
175. Vagle S, Farmer DM (1998) A comparison of four methods for bubble size and void fraction measurements. *IEEE J Ocean Eng* 23(3):211–222. doi:[10.1109/48.701193](https://doi.org/10.1109/48.701193)
176. Véron F (2015) Ocean spray. *Annu Rev Fluid Mech* 47:507–538. doi:[10.1146/annurev-fluid-010814-014651](https://doi.org/10.1146/annurev-fluid-010814-014651)
177. Violleau D, Rogers BD (2016) Smoothed particle hydrodynamics (SPH) for free-surface flows: past, present and future. *J Hydraul Res*. doi:[10.1080/00221686.2015.1119209](https://doi.org/10.1080/00221686.2015.1119209)
178. Wang H, Chanson H (2015) Air entrainment and turbulent fluctuations in hydraulic jumps. *Urban Water J* 12(6):502–518. doi:[10.1080/1573062X.2013.847464](https://doi.org/10.1080/1573062X.2013.847464)
179. Wang H, Murzyn F, Chanson H (2014) Total pressure fluctuations and two-phase flow turbulence in hydraulic jumps. *Exp Fluids* 55(11):1–16. doi:[10.1007/s00348-014-1847-9](https://doi.org/10.1007/s00348-014-1847-9)
180. Wang H, Murzyn F, Chanson H (2015) Interaction between free-surface, two-phase flow and total pressure in hydraulic jump. *Exp Thermal Fluid Sci* 64:30–41. doi:[10.1016/j.exptthermfluidsci.2015.02.003](https://doi.org/10.1016/j.exptthermfluidsci.2015.02.003)
181. Wang P, Yao Y, Tulin MP (1995) An efficient numerical tank for non-linear water waves, based on the multi-subdomain approach with BEM. *Int J Numer Methods Fluids* 20(12):1315–1336
182. Wanninkhof R, Asher WE, Ho DT, Sweeney C, McGillis WR (2009) Advances in quantifying air–sea gas exchange and environmental forcing. *Annu Rev Fluid Mech* 1:213–244
183. Wolanski E, Williams D, Spagnol S, Chanson H (2004) Undular tidal bore dynamics in the Daly Estuary, Northern Australia. *Estuar Coast Shelf Sci* 60(4):629–636
184. Wood IR (1991) Air entrainment in free-surface flows. IAHR hydraulic structures design manual No. 4, hydraulic design considerations. Balkema Publ, Rotterdam
185. Zhang G, Wang H, Chanson H (2013) Turbulence and aeration in hydraulic jumps: free-surface fluctuation and integral turbulent scale measurements. *Environ Fluid Mech* 13(2):189–204. doi:[10.1007/s10652-012-9254-3](https://doi.org/10.1007/s10652-012-9254-3)